

Stellar-mass black holes in young massive and open stellar clusters and their role in gravitational-wave generation

Sambaran Banerjee^{1,2}★

¹*Argelander-Institut für Astronomie (AIfA), Auf dem Hügel 71, D-53121, Bonn, Germany*

²*Helmholtz-Institut für Strahlen- und Kernphysik (HISKP), Nussallee 14-16, D-53115 Bonn, Germany*

October 27, 2021

ABSTRACT

Stellar-remnant black holes (BH) in dense stellar clusters have always drawn attention due to their potential in a number of phenomena, especially the dynamical formation of binary black holes (BBH), which potentially coalesce via gravitational-wave (GW) radiation. This study presents a preliminary set of evolutionary models of compact stellar clusters with initial masses ranging over $1.0 \times 10^4 M_{\odot} - 5.0 \times 10^4 M_{\odot}$, and half-mass radius of 2 or 1 pc, that is typical for young massive and starburst clusters. They have metallicities between $0.05 Z_{\odot} - Z_{\odot}$. Including contemporary schemes for stellar wind and remnant formation, such model clusters are evolved, for the first time, using the state-of-the-art direct N-body evolution program NBODY7, until their dissolution or at least for 10 Gyr. That way, a self-regulatory behaviour in the effects of dynamical interactions among the BHs is demonstrated. In contrast to earlier studies, the BBH coalescences obtained in these models show a prominence in triple-mediated coalescences while being bound to the clusters, compared to those occurring among the BBHs that are dynamically ejected from the clusters. A broader mass spectrum of the BHs and lower escape velocities of the clusters explored here might cause this difference, which is yet to be fully understood. Among the BBH coalescences obtained here, there are ones that resemble the detected GW151226, LVT151012, and GW150914 events and also ones which are even more massive. A preliminary estimate suggests few 10s-100s of BBH coalescences per year, originating due to dynamics in stellar clusters, that can be detected by the LIGO at its design sensitivity.

Key words: open clusters and associations: general – globular clusters: general – stars: kinematics and dynamics – stars: black holes – methods: numerical – gravitational waves

1 INTRODUCTION

The study of dynamical interactions of black holes (hereafter BH) in dense stellar systems is now nearly 30 years old. A key point of interest in this topic has always been the possibility of the generation of gravitational waves (hereafter GW) from dynamically-formed binary black holes (hereafter BBH). The interest in the topic has naturally got rejuvenated right after the first-time detection of GW from two BBH inspiral events by the Advanced LIGO detector, namely, the GW150914 (Abbott et al. 2016a,c), the GW151226 (Abbott et al. 2016b) and the marginal detection event LVT151012 (Abbott et al. 2016a). Generally speaking, for BBHs composed of stellar-remnant BHs such as the above detected ones, which are typically of $\sim 10 M_{\odot} - \sim 100 M_{\odot}$, the frequency of the emitted GW dur-

ing their inspiral phase falls within the LIGO’s detection band (Abbott et al. 2016a), placing such BBHs among the most promising sources for the LIGO. The bottom-line scenario of formation of dynamical (stellar-mass) BBHs in star clusters is straightforward: if a certain number of BHs receive sufficiently low natal kicks, during their formation via core-collapse (supernovae) of massive stars, that they remain bound to the gravitational potential of the cluster, they would segregate to the innermost regions of the cluster. Depending on the number of BHs retained in the cluster and their masses (which is ~ 10 to ~ 100 times the average stellar mass depending on their progenitor stars’ wind; see below), the system of bound BHs might undergo a runaway mass segregation (mass-stratification or Spitzer instability; Spitzer 1987) to form a central and highly dense subsystem of BHs, where they would continuously interact. Otherwise, the dynamical friction of the dense stellar background would as well tend to keep the BHs centrally concentrated (as these

★ E-mail: sambaran@astro.uni-bonn.de (SB)

BHs are much more massive than the normal stars, they would segregate towards the cluster’s center simply due to dynamical friction, rather than being driven by two-body relaxation).

Such a dense BH-core serves as a constant resource for dynamically forming BBH, mainly via the three-body mechanism (Spitzer 1987; Heggie & Hut 2003). The subsequent frequent and super-elastic (Spitzer 1987) dynamical encounters of a BBH with other single BHs and BBHs serve as a recipe for (a) injecting kinetic energy (K.E.) into the BH sub-cluster and as well into the whole star cluster causing the latter to expand (Mackey et al. 2007, 2008), (b) ejecting single and binary BHs from the cluster depleting the BH population and (c) forming triple-BH systems within the BH-core. The ejected BBHs are typically dynamically tightened (hardened; Heggie 1975) and also eccentric, an adequate combination of which (Peters 1964) would lead to the inspiral via GW radiation and the coalescence of a BBH within the Hubble time. The triple-BHs that are bound to the clusters, on the other hand, would typically undergo Kozai-Lidov oscillations (Kozai 1962) leading to large eccentricity boost and hence GW inspiral and coalescence of the inner binary, provided this happens before the triple gets perturbed by an intruder. In other words, although a star cluster continues to eject single and binary BHs and form BH-triples until its BH reservoir is (nearly) depleted, the occurrence of a dynamical BBH inspiral is a probabilistic phenomenon.

Beginning from 1990s, aspects of the above mechanism is studied at various levels of detail. Following preliminary but pioneering studies such as Kulkarni et al. (1993); Sigurdsson & Hernquist (1993); Portegies Zwart & McMillan (2000), more recent direct N-body (*e.g.*, Banerjee et al. 2010; Aarseth 2012; Sippel & Hurley 2013; Wang et al. 2016; Hurley et al. 2016) and Monte-Carlo (*e.g.*, Downing et al. 2010, 2011; Rodriguez et al. 2015; Morscher et al. 2015; Rodriguez et al. 2016a,b; Chatterjee et al. 2016a,b; Askar et al. 2016) calculations of model stellar clusters study the dynamically-driven depletion of BHs, the resulting feedback onto the cluster and the BBH inspirals self consistently and in much more detail. Adopting somewhat simpler but realistic conditions, detailed semi-analytic studies of these aspects have also been performed recently (Breen & Heggie 2013a,b; Arca-Sedda 2016). Also, such a semi-analytic modelling, in the context of $\sim 10^7 M_\odot$ nuclear stellar clusters and with focus on stellar-mass BBH inspirals produced by them, has been recently performed by Antonini & Rasio (2016). By nature, Monte-Carlo calculations are restricted to massive clusters, initially $\sim 10^5 M_\odot - 10^6 M_\odot$, that are more representatives (or progenitors) of classical globular clusters (hereafter GC), although young clusters of up to $\sim 10^7 M_\odot$ are observed in nearby starburst galaxies (*e.g.*, in the Antennae Larsen 2009; Johnson et al. 2015) and the impact on BBH inspiral rate due to age-spread among massive clusters has been explored very recently (Chatterjee et al. 2016b). The overall conclusion of such studies is that the dynamical BBH inspiral rate is $\approx 5 - 10 \text{ yr}^{-1} \text{ Gpc}^{-3}$, which would contribute to the detection of several 10s of BBH inspiral per year with the Advanced LIGO, given its proposed full sensitivity (Banerjee et al. 2010; Rodriguez et al. 2016a). These studies also infer that a GW150914-like BBH coalescence is intrinsically rare to

be produced from a star cluster compared to the other two events (Rodriguez et al. 2016b; Chatterjee et al. 2016b).

Another important corollary is that the BH population in massive clusters, although decays monotonically with time due to dynamical interactions, it hardly gets completely depleted even in a Hubble time, so that a substantial population of BHs would retain even in old globular clusters. In a nutshell, this is due to the energy generation via dynamical encounters in the BH-core that results in significant expansion of both the parent cluster and the BH-core itself, suppressing the BH-BH interaction rate. This “self-regulation” causes the BH population to decline but exponentially; see below and also Morscher et al. (2015). This is consistent with the recent identification of stellar-mass BH candidates in the Galactic globular clusters M22 and 47 Tuc (Strader et al. 2012; Miller-Jones et al. 2015).

The present work focuses on the other end of the problem, namely, the role of intermediate-mass and open stellar clusters in generating BBH inspirals. In this paper, by intermediate-mass clusters, we will imply those within the mass range $10^4 M_\odot - 10^5 M_\odot$, the young ($\lesssim 100 \text{ Myr}$) versions of which are popularly called “young massive clusters” (YMCs) and “starburst clusters” (when $\lesssim 4 \text{ Myr}$ old; such young clusters with $> 10^5 M_\odot$ are often denoted as “super star clusters”). Clusters of $< 10^4 M_\odot$ will be called open clusters; as such, there is no strict boundaries defined in the literature between these different “types” of clusters. A reliable and self-consistent evolutionary modelling of clusters of such masses with realistic ingredients is possible only by direct N-body integration. Monte-Carlo calculations already become unsatisfactory for the corresponding typical particle numbers ($N \lesssim 1.7 \times 10^5$), due to larger statistical fluctuations and various timescales becoming closer to the cluster’s overall two-body relaxation time.

After a recess of about a decade since a few notable initial studies on this topic (Kulkarni et al. 1993; Sigurdsson & Hernquist 1993; Portegies Zwart & McMillan 2000), Banerjee et al. (2010) have, for the first time, investigated the dynamical behaviour of a population of $\approx 10 M_\odot$ BHs in intermediate-mass compact (initial half-mass radius 1-2 pc) stellar clusters, where the dynamics of the BHs have been treated self-consistently using direct N-body calculations. As such, the above work is the first of its kind where the dynamics of the BHs in stellar clusters and the consequent impact on the cluster and the production of BBH coalescences have been studied explicitly. However, soon after, both observations of BH candidates in sub-solar metallicity regions in the Local Group and theoretical studies of the mass distribution of stellar remnants based on revised wind prescriptions for high-mass stars have suggested that stellar-remnant BHs can, in fact, be much more massive than the contemporarily accepted $\approx 10 M_\odot$ BHs, especially at low abundances (Belczynski et al. 2010). Of course, the existence of such stellar BHs is now confirmed after the GW150914 event which involves $\approx 30 M_\odot$ BHs (also by the LVT151012 event). Given the current knowledge on stellar winds in different evolutionary stages of massive stars as a function of metallicity, determining the remnant BH mass, it is likely that such $\approx 30 M_\odot$ BHs are formed in sub-solar metallicity regions (Belczynski et al. 2010; Spera et al. 2015).

Given that nearly all of the N-body studies of long-term BH dynamics in stellar clusters so far assumes $\approx 10 M_\odot$ BHs

that is representative of solar-like metallicity (Banerjee et al. 2010; Aarseth 2012; Sippel & Hurley 2013; Wang et al. 2016), it is now undoubtedly worthwhile to revisit the problem with revised BH masses. Especially, at lower metallicities, not only the stellar-remnant BHs would be substantially more massive, but also they would have a wider mass spectrum. This, in turn, would influence the nature of the dynamical interactions in a star cluster’s “BH-engine” and hence the latter’s impact on the cluster and on the BBH coalescences from it, as we will see in the following sections. Since direct N-body integration (without force softening) tracks all sorts of dynamical encounters, and particularly the close ones, with full consistency and without any assumptions, it is the ideal approach for this study. In the present work, it is for the first time that model parsec-scale intermediate-mass and open star clusters of varying metallicities are evolved using direct N-body integration from their zero-age until the Hubble time (at least for 10 Gyr). The NBODY7 code, with modified stellar mass loss and remnant formation prescriptions adopting those of Belczynski et al. (2010) are used for this purpose; that way the BH-dynamics is studied as consistently and realistically as possible now. Given the long computing times, the present set of models cover the relevant parameter space only preliminarily and thus provide limited statistics. However, they would still comprise the state-of-the-art set of N-body calculations already suggesting intriguing and new conclusions, as we shall see in the following sections. Recently, lower-mass clusters of initially $\sim 10^3 M_\odot$ are evolved, using the direct N-body method containing similar model ingredients as in here (Sec. 2.2), for shorter evolutionary times of ~ 100 Myr, to study the dynamical interactions involving BHs over young ages and low metallicities (Mapelli et al. 2013; Ziosi et al. 2014). It is also worth recalling the “Dragon Simulations” (Wang et al. 2016) in this context, where relatively extended, $\approx 3 - 8$ pc-sized, much more massive clusters of $N \approx 10^6$ stars (they can also be taken as representatives of galactic nuclear clusters) are evolved for nearly a Hubble time and the properties of the BH population are studied, through direct N-body calculations using the NBODY6++ program (Wang et al. 2015).

This paper is organized as follows: in Sec. 2, the model calculations are described (in Sec. 2.3) following a brief introduction to the NBODY7 code (Sec. 2.1) and its modifications for the present purpose (Sec. 2.2). In Sec. 3, the results of these calculations are discussed, with focus on the general dynamical behaviour of BHs and its impact on the parent cluster (Sec. 3.1), and as well on the dynamical production of BBHs and their coalescences via GW radiation (Sec. 3.2). These coalescences are compared with those detected by the LIGO (Sec. 3.2.1) and a preliminary estimate of the LIGO detection rate of dynamically-generated BBH mergers is suggested (Sec. 3.2.2). The inferences are summarized in Sec. 4.

2 MODEL CALCULATIONS

2.1 The NBODY7 N-body evolution program

The NBODY7 code is an immediate descendant of the widely-used NBODY6 direct N-body evolution code (Aarseth 2003; Nitadori & Aarseth 2012). NBODY7 utilizes the Algorithmic Regularization Chain (ARC) of Mikkola & Tanikawa (1999)

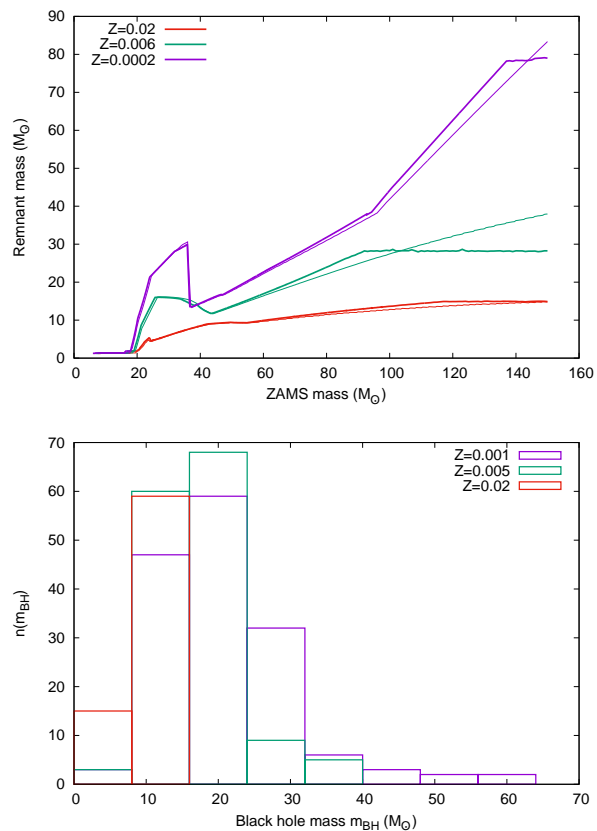


Figure 1. **Top:** Remnant mass as a function of zero-age main sequence (ZAMS) mass for the Belczynski et al. (2008, 2010) stellar wind and remnant formation schemes adopted in this study, which is obtained from the variant of BSE that is integrated with NBODY7 (thin lines). They agree reasonably well with those from B10 (thick lines) for the respective metallicities ($Z = Z_\odot, Z_\odot/4, Z_\odot/100$; see B10), which have been obtained using their StarTrack program. **Bottom:** Mass distributions of BHs that remain bound to the $M_{cl}(0) = 5 \times 10^4 M_\odot$ computed model clusters (Table 1), right after their formation, for $Z = Z_\odot, Z_\odot/4, Z_\odot/20$.

instead of the the classic Chain Regularization in NBODY6 (Mikkola & Aarseth 1993; Aarseth 2003). This enables a more thorough and reliable treatment of multiple systems that continue to form dynamically in any dense environment and influence the dynamics, especially of those involving one or more massive objects like BHs. NBODY7 otherwise follows similar numerical strategies like NBODY6, namely, a fourth-order Hermite integrator is used to accurately advance the trajectories of each star subjected to the resultant force from rest of the bodies. To ease the consequent $\propto N^3$ dependence in computing time, a neighbour-based scheme is utilized for computing the force contributions (Nitadori & Aarseth 2012) at the shortest time intervals (the “irregular” force/steps). At longer time intervals (the “regular” force/steps), all members in the system are included for the force evaluation. The inexpensive (but numerous) irregular forces are computed using parallel processing in regular single-node workstation CPUs, while the much more expensive regular force calculations are done on CUDA¹-enabled

¹ Compute-Unified Device Architecture

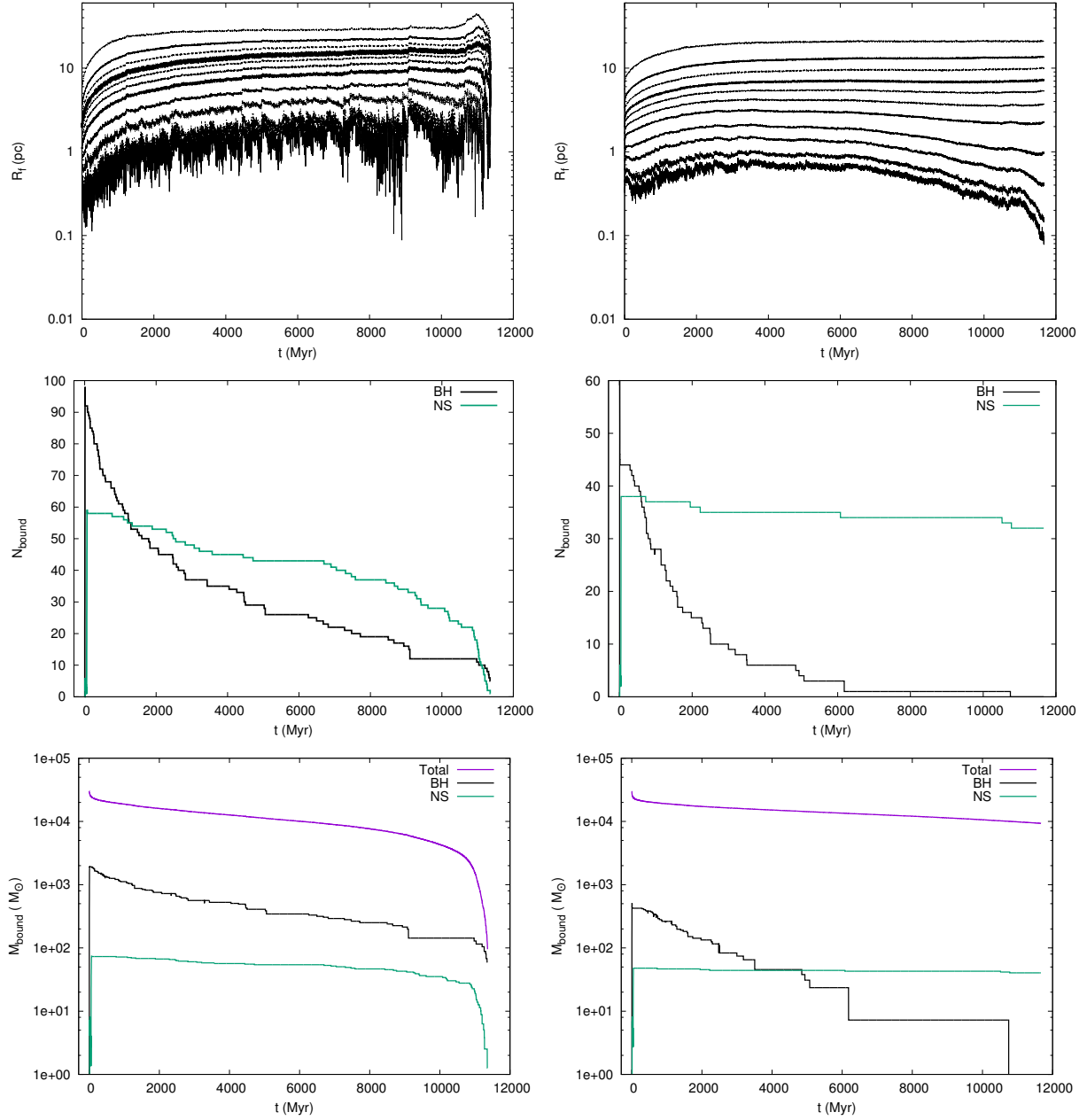


Figure 2. Examples of computed evolution, for models with $M_{cl}(0) \approx 3 \times 10^4 M_\odot$ and $r_h(0) \approx 2$ pc having metallicities $Z = 0.05Z_\odot$ (left column) and $Z = Z_\odot$ (right column); see Table 1. **Top panels:** time evolutions of the 1%, 2%, 5%, 10%, 20%, 30%, 40%, 50%, 62.5%, 75% and 90% Lagrange radii (R_f denotes the $(f \times 100)\%$ radius), **Middle panels:** evolutions of the numbers of BHs and NSs bound to the cluster, **Bottom panels:** evolutions of the total bound cluster mass (blue line) and the total masses of the BHs and NSs bound the cluster (black and green lines respectively).

high-performance GPUs². The diverging gravitational forces during close passages and in binaries are dealt with two-body or KS regularization (Aarseth 2003) and higher-order multiples are treated with the ARC.

Like its predecessors, NBODY7 utilizes the semi-analytic stellar evolution code BSE (Hurley et al. 2000, 2002)³ to

evolve each star and form their remnants. The stellar parameters of each star (including any tidal effect if it is a member of a binary or a multiple) are updated simultaneously with its trajectory integration. That way the effects

evolving single stars is called SSE, which are available as separate standalone packages. The same wind mass loss and remnant formation recipes (see Sec. 2.2) can be applied to both. In the N-body code, the evolutionary subroutines of SSE and BSE are integrated into the various NBODY7 subroutines and we will simply denote the stellar-evolutionary part of NBODY7 as BSE.

² All computations in this work are done on workstations equipped with quad-core AMD processors and NVIDIA's Fermi and Kepler series GPUs.

³ BSE is the binary stellar evolution code and its counterpart for

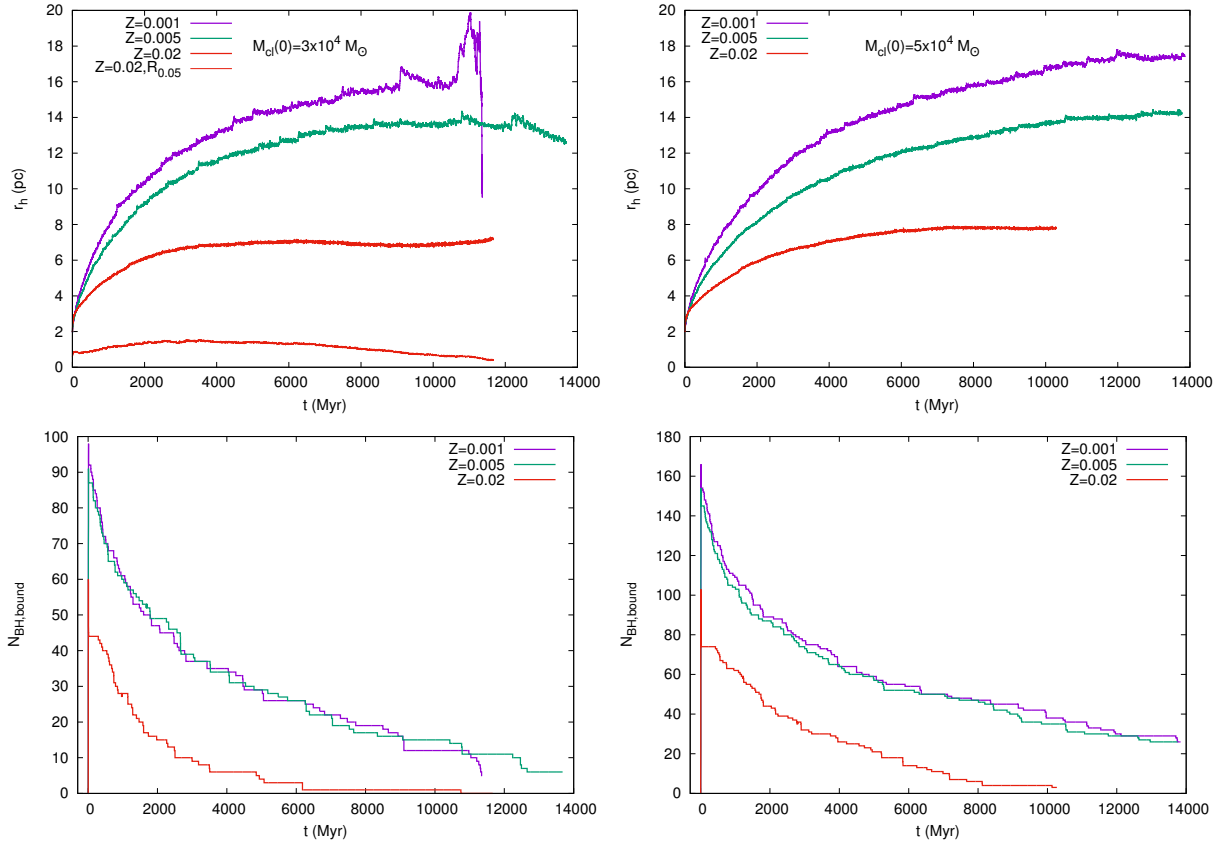


Figure 3. The time evolution of the half-mass radius (50% Lagrange radius $R_{0.5}$), r_h (top row), and the number of BHs bound to the cluster, $N_{BH, bound}$ (bottom row), as a function of metallicity, Z , for computed model clusters with $M_{cl}(0) \approx 3 \times 10^4 M_\odot$ (left column) and $M_{cl}(0) \approx 5 \times 10^4 M_\odot$ (right column), each having $r_h(0) \approx 2$ pc (see Table 1). The 5% Lagrange radius, $R_{0.05}$, is also plotted for the $M_{cl}(0) \approx 3 \times 10^4 M_\odot$, $Z = Z_\odot$ model (top left panel) to indicate that it has just arrived at its (second) core-collapsed phase.

of stellar evolutionary mass loss, via winds and supernovae, are naturally incorporated in a calculation.

An important aspect of NBODY7 is its general relativistic (GR) treatment, when an NS or/and a BH is a member of binary or a multiplet. The relativistic treatment, following the Post-Newtonian (PN) approach, is included in the ARC procedure (Mikkola & Merritt 2008). In principle, PN-1.5 (GR periastron precession), PN-2.5 (orbital shrinking due to GW radiation) and PN-3.5 (spin-orbit coupling) order terms are included in the ARC; see Aarseth (2012) for the key elements of the implementation in NBODY7 and Brem et al. (2013) for an alternative approach (in NBODY6++). This allows for on-the-fly GR orbital modifications and coalescences of relativistic subsystems (typically a binary or a triple containing one or more BH/NS) that are bound to the system. The latest implementation generally shows reasonable energy check (typical relative energy change $\sim 10^{-6}$) even during extreme relativistic events such as a BBH coalescence within a triple. In the present computations (see Sec. 2.3), however, the PN terms up to order 2.5 are applied, as activating the spin terms would make these computations, which typically contain one or more relativistic subsystems nearly all of the time, much more slower⁴. The spin terms would have modi-

fied the times of the BBH coalescences occurring within the cluster (see Secs. 1 & 3.2) to some extent, however, this is not critical in the present context due to the statistical nature of the dynamically-induced BBH coalescences.

In reality, a BBH would typically receive a substantial GW merger kick during its inspiral phase ($\sim 100 - 1000$ km s⁻¹; Campanelli et al. 2007; Hughes 2009), due to the presence of the BHs' spins. This would cause the newly-formed merged BH to escape from the cluster almost inevitably, and it would hardly have a chance to participate in dynamical encounters further. This situation is mimicked by applying a velocity kick onto the merged BH, immediately after a coalescence happens within the cluster (Sec. 3.2). To avoid large energy error, the applied kick is kept only marginally above the escape speed; ≈ 5 times the central RMS speed. This is still enough the eject the merged BH out of the cluster, in ~ 10 dynamical times; in reality a BBH coalescence product would typically escape at much higher speed⁵.

tic subsystems (a wide but eccentric BBH or a hierarchical BH-triple). This procedure is still under development and shows unstable behaviour when a large number of BHs are present (Sverre Aarseth, private communication), as in the present models, which is why the perturbed-PN has also not been applied here.

⁵ In test calculations, it is found that even if the merged product

⁴ In addition to the PN treatment in the ARC procedure, GR treatment is also applied perturbatively in case of weakly relativistic

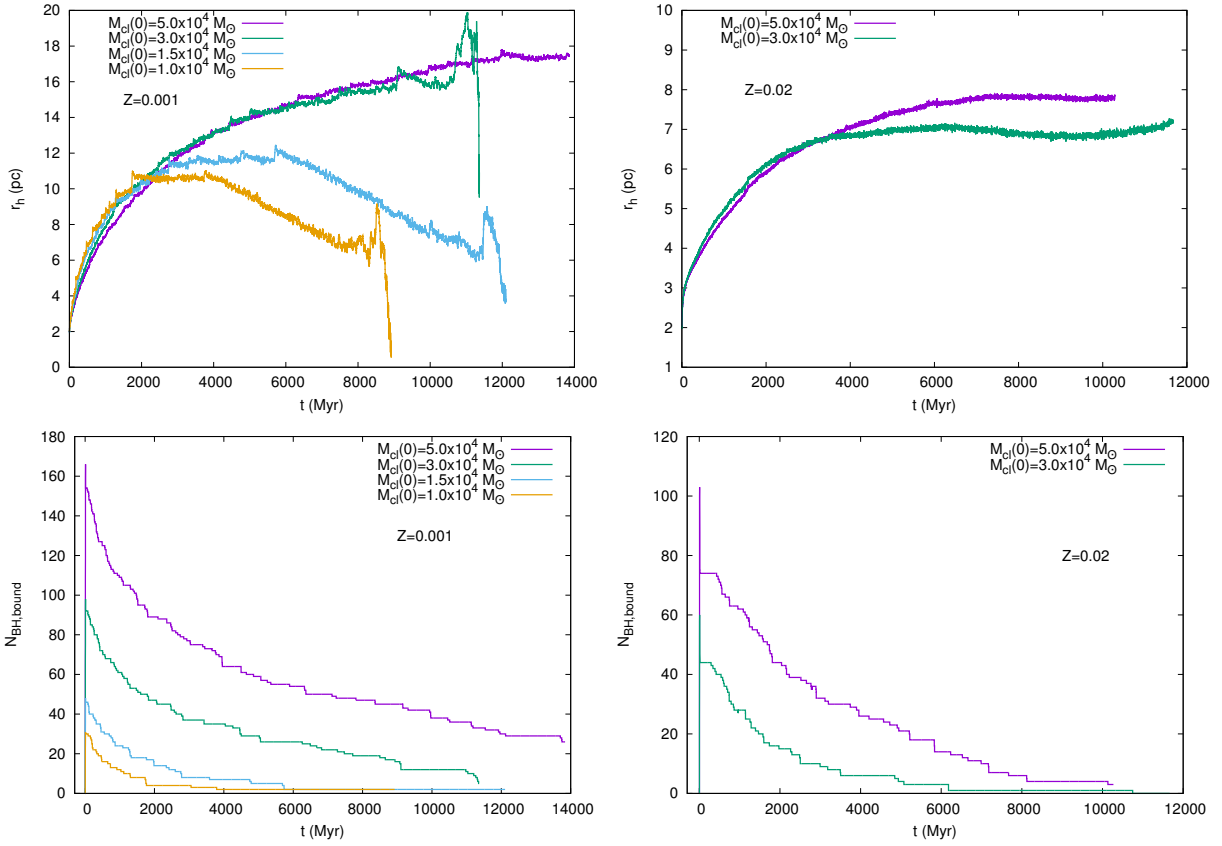


Figure 4. The evolution of r_h (top row) and $N_{BH,bound}$ (bottom row), as a function of $M_{cl}(0)$, for computed models with $Z = 0.05Z_\odot$ (left column) and $Z = Z_\odot$ (right column), each having $r_h(0) \approx 2$ pc (see Table 1).

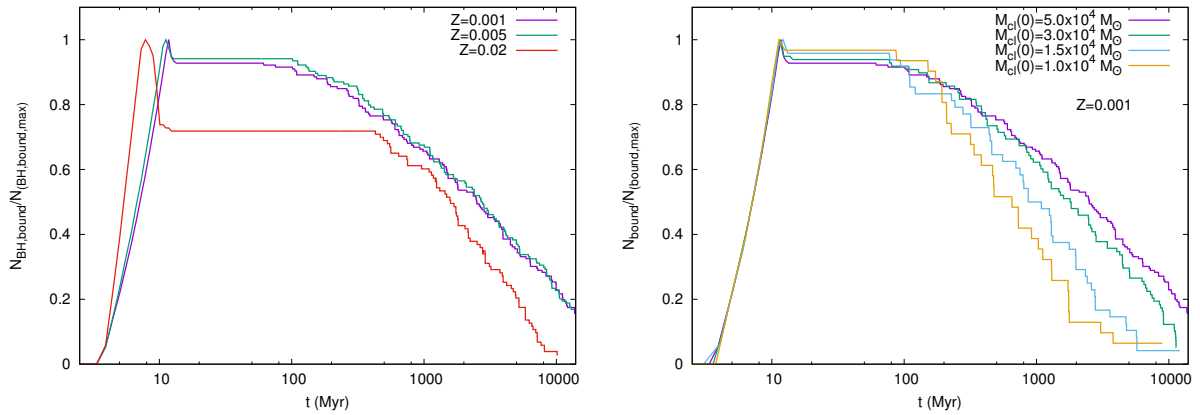


Figure 5. Left: The time evolution of the fraction of BHs bound to the cluster as a function of Z , for the computed models with $M_{cl}(0) \approx 5 \times 10^4 M_\odot$, $r_h(0) \approx 2$ pc. **Right:** The time evolution of the fraction of BHs bound to the cluster as a function of $M_{cl}(0)$, for computed models with $Z = 0.05Z_\odot$ and $r_h(0) \approx 2$ pc (see Table 1).

2.2 The new wind prescription: remnant masses and natal kicks

The masses of the BHs, and how many of them receive low natal kicks so that they can retain in the parent cluster at

is retained, it does not necessarily take part in further relativistic coalescences.

their birth, determines the effectiveness of the BH-engine (Sec. 1). For a given isolated progenitor star, the remnant BH mass is determined by the entire history of the wind mass loss until the pre-core-collapse stage and also on the material “fallback” onto the remnant during the supernova. The BH’s natal kick will be diminished by the amount of fallback; in particular there will be no natal kick if the fallback is 100%, *i.e.*, the entire pre-core-collapse star implodes into a BH (a “failed supernova”; there might still be a small kick due to

Table 1. Summary of the model stellar clusters in this work, whose evolutions are computed using `NBODY7`. The columns from left to right respectively denote: (a) initial mass, $M_{cl}(0)$, of the model cluster, (b) initial half-mass radius, $r_h(0)$, (c) metallicity, Z , (d) number of (triple-mediated) binary black hole (BBH) coalescences, $N_{\text{mrg,in}}$, that occurred within the clusters, (e) number of BBH coalescences (in BBHs ejected from the clusters), $N_{\text{mrg,out}}$, that occurred outside the clusters within the Hubble time. For the BBHs that have undergone coalescence, the masses of the corresponding binary members are indicated in parentheses in the columns (d) and (e).

$M_{cl}(0)/M_{\odot}$	$r_h(0)/\text{pc}$	Z/Z_{\odot}	$N_{\text{mrg,in}}$	$N_{\text{mrg,out}}$
5.0×10^4	2.0	0.05	1 ($24.3M_{\odot} + 17.7M_{\odot}$)	1 ($26.0M_{\odot} + 42.8M_{\odot}$)
5.0×10^4	2.0	0.25	1 ($34.5M_{\odot} + 22.7M_{\odot}$)	0
5.0×10^4	2.0	1.00	3 ($9.0M_{\odot} + 7.5M_{\odot}$) ($10.6M_{\odot} + 9.4M_{\odot}$) ($9.1M_{\odot} + 9.0M_{\odot}$)	0
3.0×10^4	2.0	0.05	1 ($38.1M_{\odot} + 25.9M_{\odot}$)	2 ($25.7M_{\odot} + 13.8M_{\odot}$) ($23.6M_{\odot} + 22.3M_{\odot}$)
3.0×10^4	2.0	0.25	0	2 ($35.2M_{\odot} + 20.3M_{\odot}$) ($15.7M_{\odot} + 12.2M_{\odot}$)
3.0×10^4	2.0	1.00	1 ($10.6M_{\odot} + 9.0M_{\odot}$)	0
1.5×10^4	2.0	0.05	1 ($49.4M_{\odot} + 30.9M_{\odot}$)	0
1.5×10^4	1.0	0.25	0	0
1.0×10^4	2.0	0.05	0	0
1.0×10^4	1.0	0.05	1 ($43.6M_{\odot} + 34.5M_{\odot}$)	0
1.0×10^4	1.0	0.25	0	0
0.7×10^4	1.0	0.05	0	0

the escape of neutrinos). If the progenitor is initially in a close binary, its mass loss (or gain) and hence the BH mass can additionally be influenced by any mass transfer or by tidal heating effect from its companion. Unfortunately, to date, massive-stellar winds, the mechanisms of core-collapse supernovae and material fallback are still poorly understood or constrained.

In this work, we will adopt the semi-analytic remnant formation and wind prescriptions of [Belczynski et al. \(2008, 2010\)](#). These rather widely used prescriptions are based on empirically-determined wind mass loss formulae of [Vink et al. \(2001\)](#) for O/B-stars, metallicity-dependent winds (including suppression due to clumping) of [Vink & de Koter \(2005\)](#) for Wolf-Rayet (naked helium) stars and metallicity-independent (suppressed) wind for Luminous Blue Variable stars; see the formulae (6)-(9) and their explanations in [Belczynski et al. \(2010\)](#) (hereafter B10). After the wind mass loss until the formation of the pre-supernova core, the remnant (NS or BH) mass is determined based on the C0 and FeNi core mass and the amount of fallback onto it as in [Belczynski et al. \(2008\)](#); see their Eqns. (1) & (2).

Such partly empirical and partly physically-motivated wind and remnant formation model combinations constitute perhaps the only known way to plausibly obtain $\approx 30M_{\odot}$ BHs as observed in the GW150914 event, at $\approx Z_{\odot}/4$ metallicity that is plausible for the Local Universe (redshift $z < 0.2$) where this event must have occurred ([Abbott et al. 2016a,c](#)). Overall, the B10 winds are much weaker at any metallicity than the standard [Hurley et al. \(2000\)](#) (hereafter H2K) winds that is adopted by default in the `BSE` (see Sec. 2.1) routine, the latter yielding up to $\lesssim 25M_{\odot}$ BHs at metallicity as low as $Z_{\odot}/100$, that is unlikely to occur in the local uni-

verse. That way the B10 wind prescription more plausibly yields the mass range of BHs inferred from the three LIGO events, than the H2K prescription (for the same [Belczynski et al. 2008](#) remnant-formation prescription), which is why the former is preferred in this study.

The birth kicks of the remnants are assigned based on their type, mass and the amount of material fallback, as derived from the above prescriptions. The NSs produced from core-collapse supernovae are given large kicks of $\approx 265 \text{ km s}^{-1}$, as inferred from observations of radio pulsars in the Galactic field ([Hansen & Phinney 1997](#); [Hobbs et al. 2005](#)). The BHs formed without or partial fallback are then assigned diminished kicks based on their final masses, that are scaled from the above NS kick assuming linear momentum conservation. For pre-supernova C0 core mass of $M_{\text{C0}} = 7.6M_{\odot}$, the fallback is taken to become complete based on the studies by [Fryer \(1999\)](#); [Fryer & Kalogera \(2001\)](#)⁶; the entire (pre-supernova) star is assumed to collapse directly into a BH for $M_{\text{C0}} \geq 7.6M_{\odot}$ when zero natal kick is assigned. NSs are also allowed to form via Electron Capture Supernovae (ECS; [Podsiadlowski et al. 2004](#)) as in [Belczynski et al. \(2008\)](#), which are of $\approx 1.26M_{\odot}$ and are as well assigned zero natal kick. For the model clusters considered in this study (with masses $M_{cl}(0) \leq 5 \times 10^4 M_{\odot}$; see Table 1), only the direct collapse BHs and ECS NSs will retain in the cluster at their birth. All core-collapse NSs and almost all other BHs will escape right after their formation, due to their high natal kicks.

⁶ In the present prescription, the fallback fraction grows linearly between $5M_{\odot} \leq M_{\text{C0}} \leq 7.6M_{\odot}$.

The above “new wind” and kick recipes have already been implemented in the `StarTrack` (Belczynski et al. 2002, 2008) semi-analytic stellar-evolutionary code and are now implemented in the `BSE`, that is integrated with the `NBODY7` (in the current version of `NBODY7`, different elements of the above wind prescriptions are available as options alternative to the default H2K recipe). As pointed out above, there are uncertainties in nearly all physical factors determining the remnant masses and their natal kicks. Therefore the presently adopted schemes can at most be taken as a physically plausible implementation of the present empirical and theoretical knowledge of stellar winds and remnant formation, which is also widely utilized (*e.g.*, in Morscher et al. 2015; Chatterjee et al. 2016a). Note that a similar wind and remnant formation schemes are adopted by Spera et al. (2015) but in a different stellar evolution and population synthesis code, namely, the `SEVN`; in this study, however, we will limit ourselves to the `BSE` as it is adapted to the `NBODY7`.

Fig. 1 (top panel) shows the remnant mass as a function of zero-age main sequence (ZAMS) mass at different metallicities, Z , as obtained by the `NBODY7`-adapted `BSE` for the presently assumed stellar wind and remnant formation recipes (thin lines). They agree reasonably well with those of B10 for the same values of Z (thick lines), which have been obtained using `StarTrack`. Fig. 1 (bottom panel) shows the mass distributions of the BHs that remain bound to the $M_{cl}(0) = 5 \times 10^4 M_{\odot}$ model clusters computed here (see Table 1) after their formation, *i.e.*, receive zero or low natal kicks (these mass distributions are obtained shortly after the last BH formed at ≈ 10 Myr, when most of the bound BHs are still segregating towards the cluster’s center but the unbound ones have already escaped through the tidal radius, and when the dynamical ejections of the BHs are yet to start; see below). As expected from the ZAMS mass-BH mass relations, lower Z would result in a wider BH mass spectrum. In all cases, only the BHs from the first mass bin are depleted due to natal kicks, the rest receive zero kicks; hence, the lower the Z is, the higher is the initial BH retention, in the present scheme.

2.3 Model computations

Table 1 lists the model computations for this study, which are done using `NBODY7`. All the computed models are initially Plummer clusters with masses $M_{cl}(0) \leq 5 \times 10^4 M_{\odot}$ and half-mass radius $r_h(0) = 2$ pc; $r_h(0) = 1$ pc are also used for a few lower mass models. Such masses and sizes are typical for Galactic and Local Group YMCs (Banerjee & Kroupa 2016; Portegies Zwart et al. 2010; Ryon et al. 2015); considering the masses of GCs, they represent intermediate-mass and open stellar clusters (see Sec. 1). From the point of view of the study of BH dynamics and dynamical BBH coalescence, such mass range is relatively unexplored (see Sec. 1 and references therein), which is alone a good reason to study them here. However, reaching higher initial masses would still have been interesting (see Sec. 3.2), and not doing so here is mainly due to the computational costs involved (most models are initiated with $r_h(0) = 2$ pc instead of 1 pc for the same reason). The initial mass function (IMF) of all the models are taken to be the canonical one, satisfying the *observed* maximum stellar mass-cluster mass relation (Wei-

ner & Kroupa 2004; Kroupa et al. 2013). The metallicities of the models are varied between $0.05Z_{\odot} \leq Z \leq Z_{\odot}$; $\approx 0.05Z_{\odot}$ being the lowest metallicity *observed* in the Local Universe (Sánchez Almeida et al. 2015; Rubio et al. 2015).

All models are evolved for 10.0-13.7 Gyr or until they dissolve completely, beginning from their zero age. A solar neighbourhood-like, static external tidal field is applied for each model. Note that this external field is just a representative in this study, whose job is simply to remove any gravitationally unbound object from the cluster’s membership, and its use is of course a simplification. In reality, a cluster would have gone through large changes in its environment over such long evolutionary times and hence in the tidal field it is subjected to (see, *e.g.*, Renaud et al. 2015); even our immediate cosmic neighborhood offers widely different environments to newly born clusters, *e.g.*, compare the external fields on to the YMCs of the Milky Way and of the Magellanic Clouds. However, the growth of the host galaxy is neither fatal to the cluster nor alters the cluster’s evolution drastically, as long as it is adiabatic (Renaud & Gieles 2015). Over most of their evolutionary time, the computed models underfill their tidal radii.

Another simplification is the assumption of a monolithic, gas-free structure of the model clusters right from their zero age, *i.e.*, neglecting their assembly phase and the effect of gas expulsion (Longmore et al. 2014; Banerjee & Kroupa 2015a). Depending on the duration of the assembly and gas dispersal phase, which, in turn, would govern the mass segregation of the massive stars and/or the stellar remnants, the dynamics of the BHs may or may not be affected significantly by the assembly process. The current assumption of a monolithic structure throughout is justified if the clusters undergo “prompt assembly” (Banerjee & Kroupa 2015b).

Finally, all the initial models contain only single stars. This is also a simplification done for the sake of computational ease. An appropriate initial binary fraction for O/B-stars would be 50%-70%, to be consistent with what is observed in starburst clusters (Sana & Evans 2011; Sana et al. 2013), which would be tedious to compute over such long evolutionary times. Recent Monte-Carlo calculations (using 5-10% O/B-stellar binary fraction; Chatterjee et al. 2016a) infer that the properties of dynamically-produced BBHs are nearly independent of the primordial binary content. This is because nearly all the BH progenitor binaries widen significantly due to stellar wind and supernova mass loss, to either get disrupted directly or get ionized by dynamical interactions with the surrounding stars, so that the majority of the BHs become single anyway. Hence, the lack of primordial binaries in our computed models would not pose a serious limitation as long as the dynamics of the BHs are concerned.

3 RESULTS

3.1 The impact of stellar-mass black holes on star cluster evolution

As outlined in Sec. 1, the primary impact of stellar-mass BH retention in a cluster just after their formation is to inject energy into the dense stellar environment due to the dynamical encounters in the BH-core (and also into the BH-core

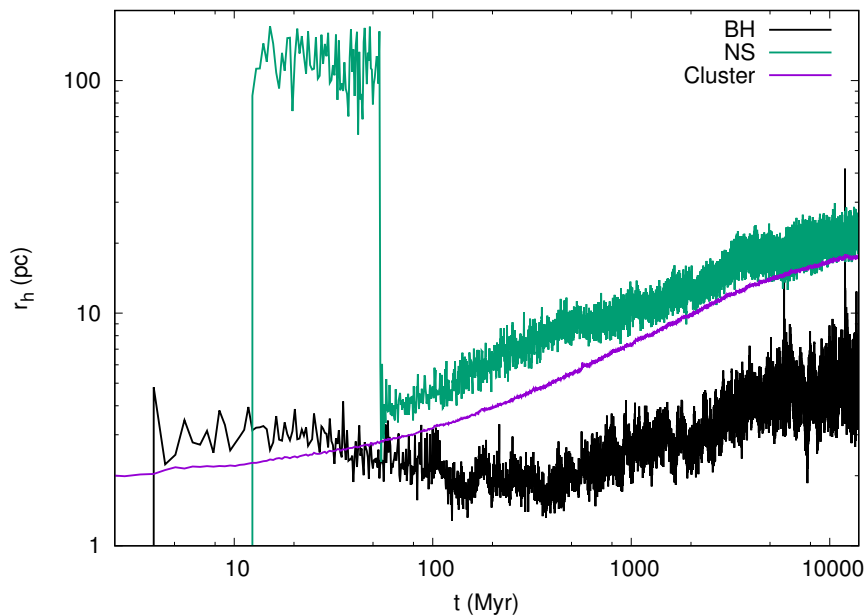


Figure 6. The time evolution of the half-mass radii of the whole cluster (blue line), the bound BHs (black line) and NSs (green line) for the computed model with $M_{cl}(0) \approx 5 \times 10^4 M_{\odot}$, $r_h(0) \approx 2$ pc, $Z = 0.05Z_{\odot}$.

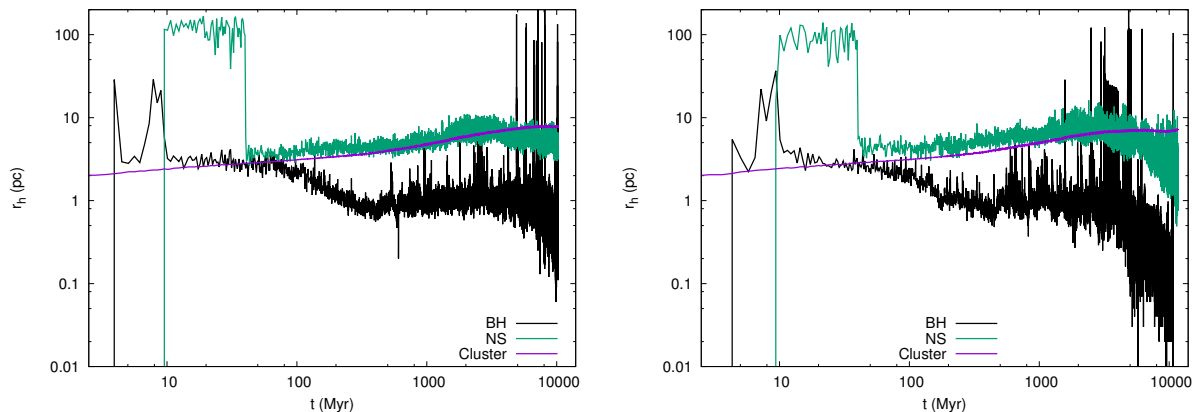


Figure 7. The same as in Fig. 6 but with $Z = Z_{\odot}$, for $M_{cl}(0) \approx 5 \times 10^4 M_{\odot}$ (left) and $M_{cl}(0) \approx 3 \times 10^4 M_{\odot}$ (right). $r_h(0) \approx 2$ pc for each.

itself). Generally, for a given mass and compactness of the parent cluster, the energy injection will be more efficient and consequently the expansion of the cluster will be larger with increasing number of post-birth retained BHs and as well with increasing mean BH mass. Both of these factors would generally boost the K.E. generated in dynamical interactions in the BH-core and the energy deposition onto the stellar environment via dynamical friction (see Sec. 1; Mackey et al. 2007, 2008). The strong and frequent dynamical encounters in the dense BH sub-cluster continue to eject BHs, mainly as single BHs and BBHs.

Fig. 2 demonstrates the evolution of $M_{cl}(0) \approx 3 \times 10^4 M_{\odot}$, $r_h(0) \approx 2$ pc models with $Z = 0.05Z_{\odot}$ and Z_{\odot} . As expected, the low- Z cluster expands by much larger extent than its solar- Z counterpart, as seen in their Lagrange-radii plots (Fig. 2, top row), due to the larger retention of the BHs at birth (both in number and total mass; Fig. 2, middle and bottom rows) in the former case. The larger rate of expansion and the

correspondingly larger rate of loss of stars across the tidal radius causes the low- Z cluster to dissolve in ≈ 11 Gyr, while the solar- Z model would survive until the Hubble time. The low- Z model also continues to retain BHs in larger number and total mass as their dynamical ejections continue (Fig. 2, middle and bottom rows); see below for more on this point. The larger BH content, in turn, continues to expand the $Z = 0.05Z_{\odot}$ cluster until its point of dissolution, while the $Z = Z_{\odot}$ cluster begins to re-collapse after ≈ 4 Gyr as its BH-engine becomes weak enough due to only a few $\approx 10M_{\odot}$ BHs remaining after this time; in fact the latter cluster undergoes (second) core collapse at ≈ 11 Gyr (*c.f.* Fig. 2, top right panel). On the other hand, the much lower-mass ECS Ns (of $\approx 1.3M_{\odot}$ each; see Sec. 2.2), that retain at birth and are yet to mass-segregate (see below), suffer a larger loss rate in the low- Z case (Fig. 2, middle and bottom rows) due to the correspondingly faster star removal.

Fig. 3 compares the time evolution of the half-mass ra-

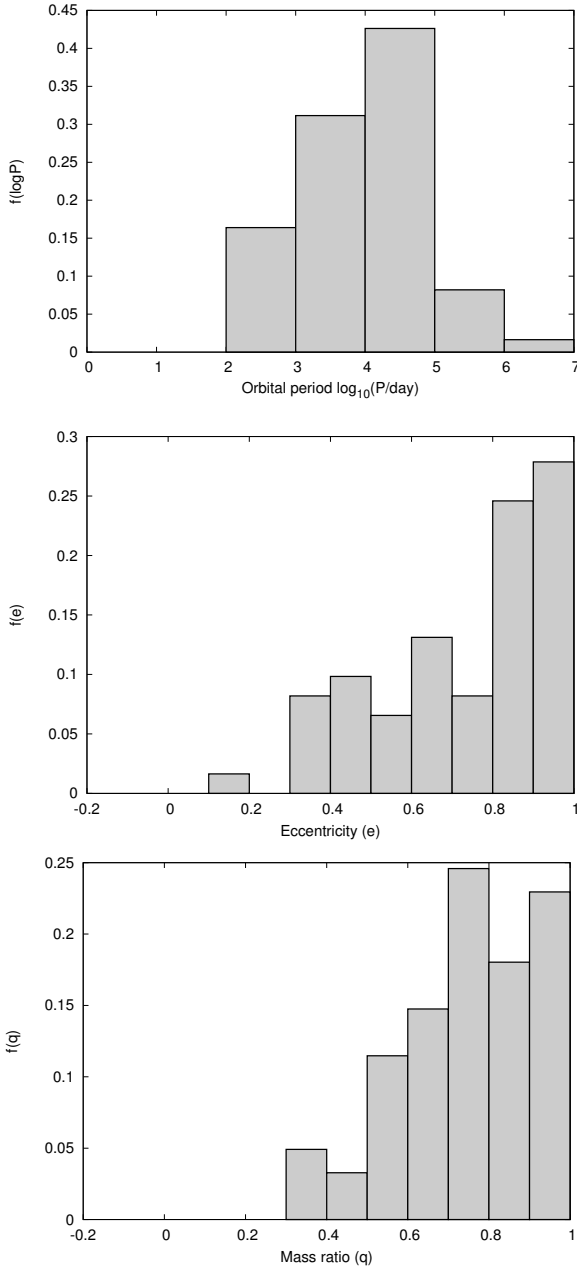


Figure 8. The distributions of orbital period (top), eccentricity (center) and mass ratio (bottom) of the dynamically-ejected binary black holes (BBHs) from all the computed models in Table 1.

dus (50% Lagrange radius), r_h , and the number, $N_{\text{BH,bound}}$, of the BHs bound (*i.e.*, those remaining within the cluster’s tidal radius; except for a few which are on their way of escaping from the cluster, they are also gravitationally bound to the system) to clusters of fixed $M_{cl}(0)$ and $r_h(0)$, but of varying Z . As can be expected based on the previous example, with decreasing Z , the by-birth retained $N_{\text{BH,bound}}$ and mean BH mass increase, causing the cluster to expand at a higher rate (Fig. 3, top row). Also, with decreasing Z , an overall larger $N_{\text{BH,bound}}$ is maintained; in fact the $N_{\text{BH,bound}}(t)$ s for $Z = 0.05Z_\odot$ and $Z = 0.25Z_\odot$ closely follow each other for most of the time while that for $Z = Z_\odot$ falls below significantly (Fig. 3, bottom row). This hints that *at least for* $Z \lesssim 0.25Z_\odot$,

the number of BHs retaining over time within a cluster of a given initial mass and size is nearly independent of Z . However, for any given observing epoch $t > 0$, a lower- Z (tidally under-full) cluster would generally be more expanded.

It would be also useful to compare $r_h(t)$ and $N_{\text{BH,bound}}(t)$, keeping Z and $r_h(0)$ fixed but varying $M_{cl}(0)$, as done in Fig. 4. Except for $M_{cl}(0) = 5 \times 10^4 M_\odot$ and $Z = 0.05Z_\odot$, which model continues to retain most BHs, the initial expansion of all clusters stall at some point when their BH-engines become weak enough due to the loss of BHs, and they begin and continue to contract until their dissolution. Because of generally smaller number (number and mean mass) of the BH content at all times, the collapse begins earlier with decreasing $M_{cl}(0)$ (increasing Z), for fixed Z ($M_{cl}(0)$) and $r_h(0)$ (also seen in Fig. 3). Note that the cluster dissolution times obtained here are exact only for the static and simplified external field assumed here (Sec. 2.3), and these times would be different under more realistic conditions.

A relevant question here is that how the *efficiency* of the dynamical BH ejection depends on $M_{cl}(0)$ and Z (for fixed $r_h(0)$)? This can be best described by plotting the time evolution of the *fraction* of the retaining BHs, as shown in Fig. 5. It can be seen that for a given $M_{cl}(0)$ and $r_h(0)$, clusters with $Z \lesssim 0.25Z_\odot$ possess nearly the same efficiency of BH ejection at all evolutionary times whereas that with $Z = Z_\odot$ is always more efficient in ejecting BHs (Fig. 5, left panel)⁷. This is counter-intuitive at the first glance, as lower Z clusters form more massive BHs and initially retain more of them in number, so that the BH-engine should become more efficient with decreasing Z . This is indeed the case: as demonstrated above, although a lower- Z cluster loses less mass over its young age from stellar winds and supernovae, it ultimately expands more and dissolves faster due to the work of its BHs. However, the larger extent of expansion and star loss causes the normal stellar density to drop faster, reducing the efficiency of dynamical friction throughout the cluster, and as well diluting the gradient of the central potential well offered by them. This causes expansion and dilution of the BH-core itself, suppressing the frequency and K.E. extraction in dynamical encounters within the BH-core, and hence its efficiency. In other words, *the BH-dynamical heating of a cluster is self-regulatory, suppressing the relative BH ejection rate for more numerous and/or more massive BH retention at birth*. This is as well manifested when Z and $r_h(0)$ are kept fixed and $M_{cl}(0)$ is varied (Fig. 5, right panel). Note that this self-regulatory behaviour is essentially a manifestation of the Hénon (1975) principle, according to which the central (dynamical) energy generation of a (post-core-collapse) cluster is controlled by the energy demands of the bulk of the cluster. This principle is as well applicable to the

⁷ In these curves, the decline of $N_{\text{BH,bound}}/N_{\text{BH,bound,max}}$ after $t \gtrsim 100$ Myr is due to the ejections of BHs via dynamical encounters. However, the drop at $t \sim 10$ Myr (distinctly visible due to the use of logarithmic t -axis) is due to the formation of BHs with relatively low natal kicks but which are still unbound w.r.t. the cluster and are removed shortly when they cross the tidal radius (see above). These are among the least massive BHs that receive the scaled natal kicks (Sec. 2.2) and which are more numerous for $Z = Z_\odot$ where the BHs have narrower mass range (Fig. 1). These BHs also cause the excursions of the BH half-mass radius evolution at $t \sim 10$ Myr in Fig. 7 (see below).

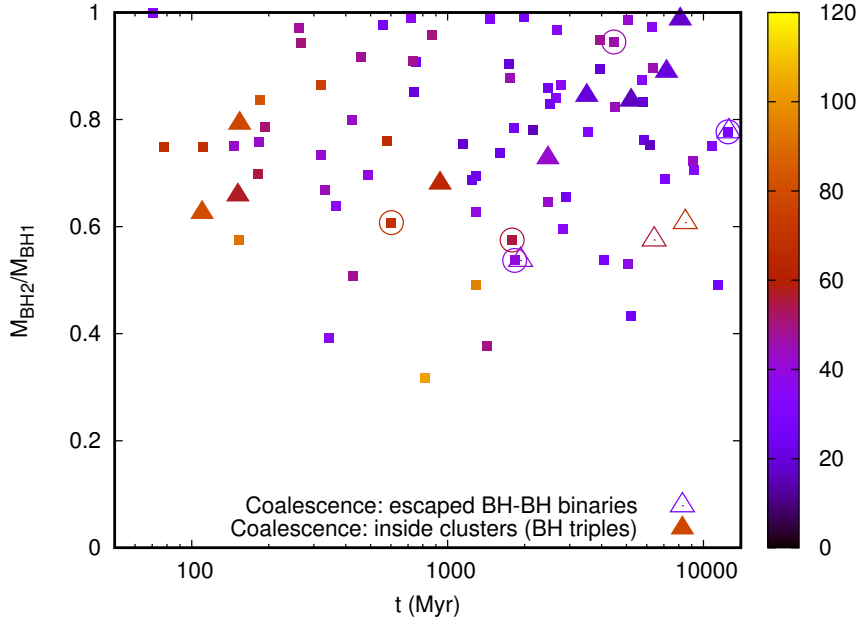


Figure 9. Filled squares: the mass ratios of the ejected BBHs against their respective cluster-evolutionary time of ejection, t_{ej} , from the model clusters. Open circles: those ejected BBHs with GW coalescence time, $\tau_{\text{mrg}} \leq 13.7$ Gyr (Hubble time) at their t_{ej} s. Open triangles: the actual times of GW coalescence, $t_{\text{mrg}} \equiv t_{\text{ej}} + \tau_{\text{mrg}}$, of the above BBHs. Filled triangles: (triple-mediated) BBH coalescences within the clusters at their corresponding coalescence times, t_{mrg} . All the symbols are colour-coded according to the BBH’s total mass, M_{tot} (vertical colour bar). Results from all the computed models in Table 1 are compiled here.

energy generation due to dynamical encounters within the BH-core inside a stellar cluster, as recently done in the semi-analytic study by Breen & Hoggie (2013a). Nevertheless, the initial retention of more numerous and/or more massive BH sub-population, ultimately injects more energy (for a given compactness) into the parent cluster (and onto itself), increasingly prolonging the BH retention, as seen from the above examples. For $M_{\text{cl}}(0) \approx 3 \times 10^4 M_{\odot}$ and $5 \times 10^4 M_{\odot}$, the $Z = Z_{\odot}$ models are nearly deprived of their BHs by 10 Gyr whereas the lower- Z models continue to hold a significant number of BHs until the Hubble time or until the cluster’s dissolution; *c.f.* Fig. 3. This result, therefore, suggests the presence of a significant population of BHs in present-day GCs as often envisaged in the literature (e.g., in Strader et al. 2012; Taylor et al. 2015; Bovill et al. 2016; Sollima et al. 2016; Peuten et al. 2016), which are typically of sub-solar metallicity, irrespective of the strength of the external field under which they orbit.

In the present context, it would be useful to also consider the ECS NSs retaining in the clusters, since in \sim Gyr old stellar systems they would be the second most massive objects. Fig. 6 compares the time evolution of the half-mass radius, $r_h(t)$, of the overall cluster with that of the half-mass radius, $r_{\text{h,BH}}(t)$, of the BH subpopulation and of the half-mass radius, $r_{\text{h,NS}}(t)$, of the NS subpopulation, for the $M_{\text{cl}}(0) \approx 5 \times 10^4 M_{\odot}$, $r_h(0) \approx 2$ pc, $Z = 0.05 Z_{\odot}$ model. After the initial central segregation of the BHs in ≈ 100 Myr, the BH-core could maintain a fluctuating but overall constant size for a few 100 Myr and then it expands with the cluster (see discussion above) until the Hubble time, $r_{\text{h,BH}}(t)$ being always a factor of few smaller than $r_h(t)$. This implies a continued centrally-concentrated (or BH-core) state of the BH sub-population within the cluster, despite significant dilu-

tion of both with time. On the other hand, $r_{\text{h,NS}}(t) > r_h(t)$ always, especially for $t \gtrsim 50$ Myr, which implies lack of mass segregation of NSs throughout the evolution. The initial large overshoot of $r_{\text{h,NS}}(t)$ is due to the formation of NSs via core-collapse supernovae that gives them large kicks (see Sec. 2.2) and they are more likely found much outside the cluster but within the tidal radius (~ 100 pc at that time), while escaping the system. The low-kick ECS NSs are born during $t \approx 56.1 - 65.3$ Myr ($t \approx 40.2 - 46.0$ Myr) for $Z = 0.05 Z_{\odot}$ ($Z = Z_{\odot}$) whose progenitors, of $\approx 6.8 - 6.3 M_{\odot}$ ($\approx 8.2 - 7.7 M_{\odot}$) ZAMS, could not yet fully segregate and, in fact, the large mass loss until the remnant formation (the ECS NSs are only of $\approx 1.3 M_{\odot}$) is likely to reverse any partial segregation achieved by their progenitors. The central K.E. injection, due to the initial rapid segregation of the retaining BHs and the continued energetic dynamical encounters among them thereafter (see above), quenches the “natural” two-body relaxation driven mass-segregation within the cluster, including that of the NSs. In the example of Fig. 6, the mass segregation is frozen until the Hubble time. For models of higher Z , where the BH-engine is weaker and the BHs are depleted relatively fast (see above), the mass segregation can revive; this is demonstrated in the $Z = Z_{\odot}$ examples in Fig. 7 where the $r_{\text{h,NS}}(t)$ falls below $r_h(t)$ after a few Gyr of evolution. Such stalling of mass segregation, due to the work of BHs, has also been demonstrated in the recent studies by Alessandrini et al. (2016); Peuten et al. (2016).

3.2 Dynamically-formed binary black holes: gravitational-wave coalescence events

Given the current interest in BBH coalescence events following their detection by the LIGO, it is undoubtedly worth-

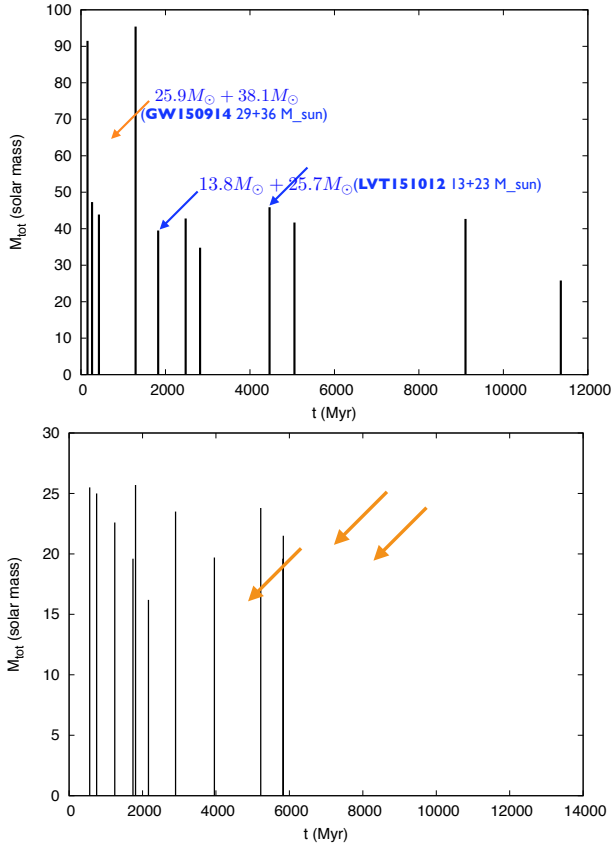


Figure 10. **Top:** the M_{tot} s of the ejected BBHs against their corresponding t_{ej} s for the computed model with $M_{cl}(0) \approx 3 \times 10^4 M_{\odot}$, $r_h(0) \approx 2$ pc, $Z = 0.05 Z_{\odot}$. The ejected BBHs with $\tau_{\text{mrg}} \leq 13.7$ Gyr are indicated by the blue arrows and the BBH coalescence within the cluster is indicated by an orange arrow; *c.f.* Table. 1. The BBH coalescences, that resemble the LIGO-detected ones (see Sec. 1) in terms of their component masses, are indicated. **Bottom:** same as the top panel but for the model with $M_{cl}(0) \approx 5 \times 10^4 M_{\odot}$, $r_h(0) \approx 2$ pc, $Z = Z_{\odot}$. All the BBH coalescences occur within the cluster, in this particular model; *c.f.* Table. 1.

while to investigate such events in the present model computations. This is of enhanced interest in this work, since YMCs and open-type clusters are dealt with here. If a power-law shape of the new-born clusters’ mass function can be assumed for throughout the Universe, as observed in our nearby spiral and starburst galaxies (typically of index $\alpha \approx -2$, Gieles et al. 2006a,b; Larsen 2009), such clusters will be the most abundant ones, among those that survive for at least a few Gyr. Therefore, although expected to be lower than GCs per cluster, their overall contribution to the observable BBH inspiral rate in the Universe could be at least comparable to that from classical GCs, thereby potentially adding significantly to the BBH detection rate from the dynamical channel. This question remains rather unexplored until now.

All the models computed here continue to eject BBHs, which can quench only when 1 or 2 BHs remain bound (in the $M_{cl}(0) \approx 3 \times 10^4 M_{\odot}$, $Z = Z_{\odot}$ model, even the final BH is ejected dynamically when the central density is increased, as the cluster approached core collapse, although such complete depletion of BHs is generally unlikely; see Fig. 2).

However, the total number of ejected BBHs per cluster is much smaller than that is typical for more massive Monte-Carlo based models (see Sec. 1 and references therein), as expected. Fig. 8 gives the distributions of orbital period, P , eccentricity, e , and mass ratio, q , for the escaped BBHs from all computed models combined. The majority of these BBHs have $P \sim 10^4 - 10^5$ days⁸. As characteristic of dynamically ejected binaries (via close encounters), the ejected BBHs are generally of high eccentricity, with the e -distribution peaked beyond $e > 0.8$. The mass ratios of the ejected BBHs are typically of $q > 0.5$, with the q -distribution function increasing towards $q = 1$. This feature of the q -distribution is a signature of the dynamical formation of the BBHs within the cluster before getting ejected, in which process the pairing of BHs of comparable masses is energetically favourable.

Except for the least massive ones, all cluster models computed here have produced BBHs that coalesce within a Hubble time (beginning from the clusters’ zero age) due to GW emission, either still being bound to the cluster (which would typically occur due to Kozai mechanism in BH-triples; see Sec. 1) or being among the escaped BBHs. The second-last column in Table. 1 shows the number, $N_{\text{mrg,in}}$, of BBH coalescences that occurred within each of the model clusters and also the corresponding component BH masses. The final column in Table. 1 gives, for each model, the number of ejected BBHs, $N_{\text{mrg,out}}$, and their component masses, that have GW merger time, $\tau_{\text{mrg}} < 13.7$ Gyr (Hubble time), at the time of ejection. Note that the bound-to-the-cluster coalescences happen in the computations on the fly (see Sec. 2.1), whereas, for the BBHs ejected from the clusters, the corresponding τ_{mrg} s are estimated using the standard orbit-averaged GW-shrinkage formula by Peters (1964).

An interesting fact, that immediately becomes apparent from Table 1, is that, in general, $N_{\text{mrg,in}} > N_{\text{mrg,out}}$, for models with $M_{cl}(0) > 10^4 M_{\odot}$. In other words, *YMCs and their derivative open clusters (as they evolve), are inherently more efficient in producing in-cluster, triple-mediated BBH coalescences than through ejecting BBHs*. This is in contrast to what Monte-Carlo calculations of much more massive systems but with similar model ingredients find (see, *e.g.*, Morscher et al. 2015; Rodriguez et al. 2016a; Chatterjee et al. 2016a). This difference could be due to artefacts in the Monte-Carlo treatment itself, especially how multiple systems are treated there. On the other hand, this could as well be characteristic of the lower-mass systems that is dealt with here; because of lower density of stars and BHs in the present models, the dynamically-formed triples can last unperturbed for longer time, giving higher chance to their inner binaries to merge via Kozai oscillations. This becomes further apparent from the fact that for the models with $M_{cl}(0) \leq 1.5 \times 10^4 M_{\odot}$, BBH coalescences occur only within the clusters (*c.f.* Table. 1).

⁸ The majority of the ejected BBHs are from the $M_{cl}(0) \approx 3 \times 10^4 M_{\odot}$ and $5 \times 10^4 M_{\odot}$ clusters and hence the P -distribution and, particularly, its peak are more of the characteristics of the ejected BBHs from these clusters. Lower-mass clusters would generally eject wider BBHs and vice versa. The low number of ejected BBHs per cluster here makes the comparison among the BBH distributions corresponding to different $M_{cl}(0)$ s and Z s less meaningful, which is otherwise advisable.

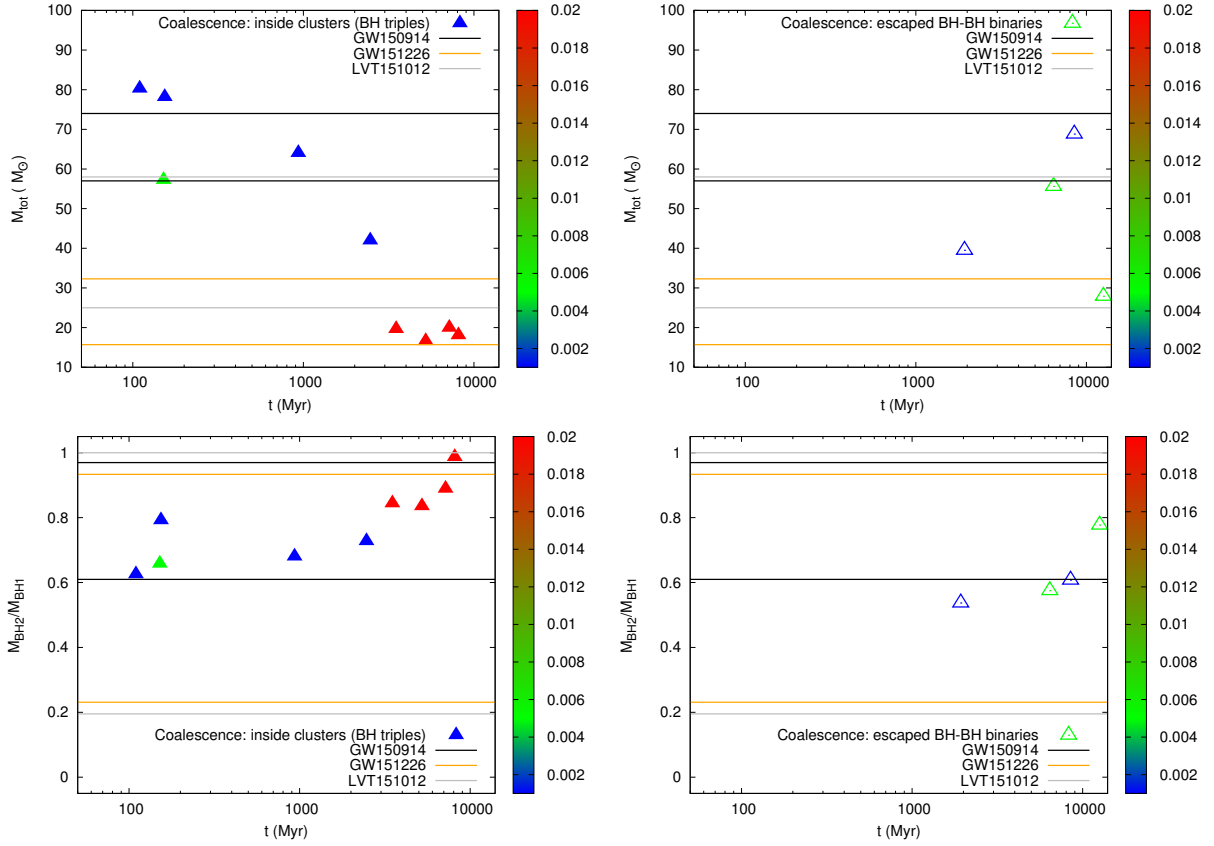


Figure 11. Top panels: the M_{tot} s of the in-cluster (triple-mediated; left) and the ejected (right) BBH coalescences against their corresponding t_{mrg} s, for all the computed models in Table 1. The colour-coding is according to the parent model cluster’s Z (vertical colour bar). **Bottom panels:** the above BBHs plotted with their mass ratios in the Y-axis. In all the panels, the ranges in the Y-axis corresponding to the detected BBH coalescence events are indicated by the horizontal lines.

Interestingly, such prominence of in-cluster BBH coalescences, as seen here, also contrasts the results obtained from earlier direct N-body calculations of models of similar mass and size containing $\approx 10M_{\odot}$ BHs, where the escaped BBH coalescences typically dominated over the in-cluster ones; see, *e.g.*, Banerjee et al. (2010). This is likely to be the result of a much broader BH mass distribution in the present models. The most massive couple of BHs would favourably become binary pair within the dense BH-core which would tend to prevent less massive BHs to pair, and would eject them preferably as singles via super-elastic scattering. This would suppress the number of ejected BBHs for a given (initial) mass and size of the cluster, and hence the coalescences among them. At the same time, the “bully” BH-binary, which would typically be the most massive object in the system, would be harder to eject dynamically, giving it enhanced opportunity to coalesce (or induce coalescence), if at all, within the cluster. In contrast, in a BH-core comprising of equal-mass or nearly equal-mass BHs, as in several previous studies, the dominance of a single BH pair would no more be energetically favourable, which would reverse the situation. To understand the role of (triple-induced) BBH coalescences within the cluster, it is necessary to do N-body calculations as in here in larger numbers and with even higher $M_{\text{cl}}(0)$, which is planned for the near future (see also Kimpson et al. 2016; Haster et al. 2016 in this context).

The filled squares in Fig. 9 indicate the mass ratios (qs) of the ejected BBHs from all the models computed here against their respective ejection times (t_{ej} s), which symbols are colour-coded according to their total masses, M_{tot} . The qs corresponding to the in-cluster and after-ejection BBH coalescences are highlighted (by filled and empty triangles respectively) at the times, t_{mrg} , of their occurrences (therefore, for the ejected BBH coalescences, $t_{\text{mrg}} \equiv t_{\text{ej}} + \tau_{\text{mrg}}$). As already indicated by Fig. 8 (bottom panel), most ejected BBHs and all BBH coalescences have $q > 0.5$. In-cluster coalescences can happen from as early as $t_{\text{mrg}} \sim 100$ Myr until ~ 10 Gyr; more massive of those ($60M_{\odot} \lesssim M_{\text{tot}} \lesssim 80M_{\odot}$) typically happening within $t \lesssim 1$ Gyr. On the other hand, in the present sample, all coalescences among the ejected BBHs happen after $t \gtrsim 1$ Gyr (including their t_{ej} s). Note that the latter conclusion can be an artefact of the low number of (only 4) ejected coalescences within the Hubble time (see Fig. 9); single BHs and BBHs begin to get ejected as soon as the central BH sub-cluster becomes concentrated enough that three-body binaries start forming in them (see Sec. 1; this is also when the contraction of the BH sub-population stalls, see, *e.g.*, Fig. 6), from $t \sim 100$ Myr.

3.2.1 Comparison with the detected binary black hole coalescences

It would undoubtedly be useful to compare the LIGO-detected events with the BBH mergers from the present set of computations. Fig. 10 plots the M_{tot} s of the ejected BBHs vs. their t_{ej} s for the $M_{\text{cl}}(0) \approx 3 \times 10^4 M_{\odot}$, $r_h(0) \approx 2$ pc, $Z = 0.05 Z_{\odot}$ model (top panel) and the $M_{\text{cl}}(0) \approx 5 \times 10^4 M_{\odot}$, $r_h(0) \approx 2$ pc, $Z = Z_{\odot}$ model (bottom panel). The ejected BBHs with $\tau_{\text{mrg}} < 13.7$ Gyr are indicated (blue arrows) and as well any coalescences within the clusters (orange arrows). Remarkably, two mergers in the $M_{\text{cl}}(0) \approx 3 \times 10^4 M_{\odot}$ cluster resemble the events GW150914 and LVT151012, both in terms of their M_{tot} s and also in individual component masses (Sec. 1 and references therein).

The $M_{\text{cl}}(0) \approx 5 \times 10^4 M_{\odot}$ run is also remarkable in the sense that it has produced 3 BBH coalescences, all within the cluster and between $5 \lesssim t \lesssim 8$ Gyr, when nearly 3/4th of its initially-retained BHs have already escaped (see Fig. 3, lower-right panel). All the mergers are of GW151226-type, in terms of their M_{tot} s. This particular calculation is unique among the set in this study, where the lower mass $\approx 10 M_{\odot}$ BHs (since $Z = Z_{\odot}$) allowed the cluster, and hence the BH sub-cluster (see Sec. 3.1), to remain sufficiently concentrated throughout its evolution. In particular, the cluster and its BH-core begin to collapse and boost their concentrations after $t \approx 3$ Gyr (see Fig. 7, left panel), with a sufficient number of BHs (≈ 20) still retaining to continue forming BH-triples which are relatively uninterrupted. The BHs, in this case, are similarly massive which favour dynamical BBH formation (see above) and hence the formation of BH-triples within the core. This implies that *intermediate-aged massive open clusters of solar-like metallicity serve as highly potential sites for dynamically generating GW151226-like BBH coalescences*. Similar calculations over a wider parameter range is necessary to reassure this intriguing inference⁹.

Fig. 11 shows the M_{tot} s (top row) and qs (bottom row) of the in-cluster (left column) and escaped (right column) BBH coalescences, at their respective t_{mrg} s, from the present set of computations, which are compared with the limits of the detected events. All the symbols here are colour-coded according to the parent cluster's Z . As already seen above, the in-situ mergers occur from age as young as $t \approx 100$ Myr up to at least 10 Gyr. Typically, lower Z clusters yield more massive coalescences, which occur at earlier t_{mrg} (the negative trend in Fig. 11, top-left panel). This overall trend is due to the fact that more massive BHs segregate and interact dynamically earlier (see also Chatterjee et al. 2016b in this context). The qs of all in-situ BBH coalescences are > 0.6 (Fig. 11, bottom-left panel), since pairings within the cluster would preferably happen among BHs whose masses are close to each other (see above). The lower-mass BHs, which are dynamically processed later in time, are likely to have partners that are closer in mass (due to the IMF slope and the BH mass-ZAMS mass relation; see Sec. 2.2), giving rise to the positive trend of the in-situ mergers' qs with t_{mrg} (Fig. 11,

bottom-left panel). A similar trend follows for the qs of the escaped BBH coalescences; however, all the escaped coalescences happen after ≈ 1 Gyr (Fig. 11, bottom-right panel). Also, the escaped coalescences generally have lower qs than their in-cluster counterparts. There is no particular trend seen in the M_{tot} s of the escaped BBH coalescences (Fig. 11, top-right panel) which is likely to be an artefact of the low number of them, in the present sample.

According to Fig. 11, all of the clusters computed here have the potential to give rise to BBH coalescence events resembling the detected ones, by dynamical means. All of the detected events could have occurred either in-situ or after being ejected from their parent clusters. Finally, at the time of the coalescence, their parent cluster could either be a ~ 100 Myr YMC (likely, if the event is in-situ) or be a few - 10 Gyr old intermediate-mass cluster/open cluster (likely for both in-situ and ejected events). Interestingly, BBH coalescences, with M_{tot} exceeding the upper limit of GW150914 by $\approx 10 M_{\odot}$, are also produced in the present computations, as seen in Fig. 11 (top-left panel). In fact these two in-cluster mergers take place the earliest ($t_{\text{mrg}} \sim 100$ Myr) and in the least massive clusters ($M_{\text{cl}}(0) \approx 1.0 \times 10^4 M_{\odot}$ and $1.5 \times 10^4 M_{\odot}$; see Table 1). The lower velocity dispersion in the BH-core of such lower-mass systems would typically produce wider BBHs via three-body encounters, causing an overall weaker energy extraction in the BH-core and, thereby, making it harder for the most massive BHs to get ejected (although they begin to participate in the dynamical interactions the earliest); such clusters are otherwise most efficient in ejecting BHs, in the sense of Fig. 5 (right panel). This, combined with such clusters' shorter BH-segregation timescale and shorter two-body relaxation time of the BH-core, have resulted in such early and massive BBH coalescences. *If BBH coalescences, substantially more massive than GW150914 (by $\sim 10 M_{\odot}$), are detected by the Advanced LIGO in the future, $\sim 10^4 M_{\odot}$, low-metallicity, compact YMCs would be potential sites for them.*

In making such comparisons, one should bear in mind the cosmological aspects of it. To detect an event today, one should take into account the time, t_{mrg} , for the BBH coalescence to occur, counting from the zero age of the parent cluster, plus time light travel time, t_L , for the merger GW signal to reach us from the location of the event. At its design sensitivity, the Advanced LIGO would detect the inspiral signal from a pair of $10 M_{\odot}$ BHs from maximum $D_{10} \approx 1500$ Mpc (comoving radial) distance (see, e.g., Banerjee et al. 2010), which corresponds to a redshift of $z \approx 0.37$ and a light travel time of $t_L \approx 4.2$ Gyr¹⁰ (Wright 2006). For a pair of $40 M_{\odot}$ BBH coalescence (the most massive ones here; c.f. Table 1), the limiting distance is $D_{40} \approx 4800$ Mpc (Eqns. 6 & 7 of Banerjee et al. 2010), corresponding to $z \approx 1.68$ and $t_L \approx 9.9$ Gyr. If the trends seen in Fig. 11 can be bought as a rough representative, then *clusters of all ages can, in principle, be parents of the detected BBH merger events, depending on the epochs of their formation*. However, the details of the cosmology must be taken into account to properly estimate the detection rate of BBH coalescences (see, e.g., Belczynski et al. 2016; Chatterjee et al. 2016b), which is beyond the scope of this article.

⁹ GCs, however, may not be as suitable for creating such a scenario, due to their much longer two-body relaxation time, which would cause the re-collapse phase to proceed much slower. However, they would be more efficient in producing GW151226-like coalescences from ejected BBHs.

¹⁰ Here we assume $h = 0.677$, $\Omega_M = 0.309$, flat Universe.

3.2.2 LIGO detection rate of binary black hole mergers: a preliminary estimate

It would still be useful to make a preliminary estimate of the GW-inspiral detection rate from dynamically-generated BBH coalescence events, by the LIGO at its design sensitivity, based on the qualitative aspects learnt from the present computations. We will assume that all the stellar clusters, contributing to the BBH mergers intercepted at the current epoch, are formed ≈ 10 Gyr ago (which is not necessarily true), *i.e.*, they would currently be either low- Z GCs or low- Z open clusters, if they still survive. Unlike in Banerjee et al. (2010), where it is assumed that nearly all BHs will be depleted by ≈ 3 Gyr of cluster evolution and also that most BBH mergers happen over this time period (based on the results from those calculations), typically a significant number of BHs continue to retain until the Hubble time or until dissolution, for low- Z systems, as seen in the present calculations (Sec. 3.1). Also, except for the least massive systems considered here, all clusters tend to produce BBH mergers (either in-situ or ejected) over all evolutionary ages (Sec. 3.2). Hence, not only the intermediate-aged clusters, but also the classical GCs of the Universe would actively contribute to present-day BBH mergers. Therefore, here we can take, as the space density of clusters, ρ_{cl} , the sum of those of both GCs and “young populous clusters” (Portegies Zwart & McMillan 2000), *i.e.*,

$$\rho_{cl} = 11.9h^3 \text{ Mpc}^{-3},$$

which would contribute to the present-day BBH mergers.

To estimate a bare minimum rate, we will consider the spherical volume of radius D_{10} (see Sec. 3.2.1), from within which essentially any BBH coalescence is, in principle, detectable by the LIGO, at its design sensitivity. If we conservatively assume only one BBH merger event per cluster, over the corresponding $t_L \approx 4.2$ Gyr (see Sec. 3.2.1), then the corresponding LIGO detection rate would be $R_{\text{LIGO}} \approx 13 \text{ yr}^{-1}$. Over D_{40} , this rate would scale up to $R_{\text{LIGO}} \approx 425 \text{ yr}^{-1}$. However, the latter rate is an overestimation since not all BBH inspiral signals can be detected by the LIGO, from distances beyond D_{10} , even at its full sensitivity. Instead, if one modestly assumes only one BBH inspiral per cluster over 10 Gyr (which time is close to the t_L from D_{40}), that can be detected by the LIGO from within the D_{40} limiting distance, then $R_{\text{LIGO}} \approx 170 \text{ yr}^{-1}$, at the design sensitivity. Of course, larger contribution per cluster and contributions from clusters that are formed at later epochs, would increase both of the limits of R_{LIGO} . Based on the above preliminary estimates, it can generally be taken that R_{LIGO} , due to dynamical BBH coalescences, would lie between few 10s to few 100s per year, at the LIGO’s design sensitivity. A more elaborate evaluation of R_{LIGO} is planned for the near future.

4 SUMMARY AND OUTLOOK

The model cluster computations presented in this work, although comprise a preliminary set but with realistic ingredients (Secs. 2.1 & 2.2), provide new and intriguing inferences. They span an initial mass range of $1.0 \times 10^4 M_{\odot} \lesssim M_{cl}(0) \lesssim 5.0 \times 10^4 M_{\odot}$, a metallicity range of $0.05Z_{\odot} \leq Z \leq Z_{\odot}$ and are of half-mass radius $r_h(0) \approx 2$ pc; for models of $M_{cl}(0) \lesssim 1.5 \times 10^4 M_{\odot}$, $r_h(0) \approx 1$ pc is also assumed. All models

are evolved by direct N-body method until their dissolution or otherwise at least for 10 Gyr. This allows one to study and compare YMC-like systems of varying Z , which evolve into open cluster-like systems, especially w.r.t. the role of stellar-mass BHs and the dynamically-triggered BBH coalescences. This mass range has not yet been explored in this way, although more massive GC-like systems have been studied often (Sec. 1 and references therein).

The BHs that form by direct collapse receive no birth kick and remain bound to the parent cluster right after their formation (Sec. 2.2). The initially-retained BHs segregate to the cluster center in ~ 100 Myr, where they form a dense BH sub-cluster. The frequent and energetic dynamical encounters in this BH-engine (or BH-core) continue to inject energy into the dense normal-stellar bulk of the cluster, until the majority of the BHs are ejected via the strong dynamical encounters. The energy injection causes the parent cluster to expand, until the BH-engine is sufficiently weakened due to the depletion of BHs, after which the cluster begins to re-collapse (Sec. 3.1; Figs. 3 & 4). The BH-core also acts to “freeze” the otherwise natural two-body relaxation-driven mass segregation process (*e.g.*, that of the ECS NSs), which can resume only after most of the BHs are dynamically depleted (Figs. 6 & 7). Lower- Z clusters would retain more massive and larger number of BHs at birth (Sec. 2.2; Fig. 1), which would have a more profound effect on the cluster. However, the energy injection process by the BHs seems to be self-regulatory: the more powerful BH-engine for a lower- Z system also acts to moderate the dynamical BH ejection, causing a larger fraction of BHs to be retained with time (Sec. 3.1; Fig. 5). As a result, the sub-solar- Z clusters computed here still retain ~ 10 BHs until the Hubble time or until shortly before their dissolution, whereas their solar- Z counterparts are nearly deprived of their BHs by similar evolutionary times (Fig. 3).

All of the computed models of masses $M_{cl}(0) \approx 5 \times 10^4 M_{\odot}$ and $\approx 3 \times 10^4 M_{\odot}$ and the lowest- Z ones of masses $M_{cl}(0) \lesssim 1.5 \times 10^4 M_{\odot}$ produce BBH coalescences due to inspiral via GW radiation (Sec. 3.2; Table 1). They occur either via Kozai mechanism in the dynamically-produced BH-triples that are bound to the cluster or among the dynamically-ejected eccentric BBHs. For the present set of models, the majority of the BBH mergers happen triple-mediated, within the parent cluster. This is in contrast with earlier N-body calculations that contained BHs of masses similar to each other and also with Monte-Carlo calculations of more massive clusters having similar model ingredients as the present ones (see Sec. 3.2 and references therein). Given that dynamically-formed subsystems are treated naturally and accurately in direct N-body calculations (Sec. 2.1), this is unlikely to be an artefact of the numerical methods applied here. As explained in Sec. 3.2, a much broader mass spectrum of the BHs is likely to favour in-situ BBH coalescences, at least over the mass range of the clusters computed here. It is important to reach even higher $M_{cl}(0)$ s using the direct N-body method, to properly understand the role of BH-triples and also the differences with the Monte-Carlo models and with the previous N-body models. Because of dynamical pairing, most of the BBHs and their coalescences have mass ratio $q > 0.5$ (Sec. 3.2; Fig. 9). Among the coalescences obtained here, there are ones which resemble well with one or other of the events detected by the LIGO until now (Sec. 3.2.1; Figs. 10 &

11). Interestingly, the lowest massive clusters computed here have produced the most massive and the earliest (in-situ) BBH coalescences, that well exceed the M_{tot} of GW150914; this might be a result of weaker dynamical encounters in these systems combined with their shorter relaxation times (see Sec. 3.2.1). Again, a larger number of such lower-mass, low- Z model computations is necessary to ascertain this, and to understand it better. A back-of-the-envelope conservative estimation is that, under its proposed design sensitivity, the LIGO should detect ~ 10 – ~ 100 BBH inspiral events per year, due to dynamical interactions among stellar-mass BHs in star clusters alone (Sec. 3.2.2).

The primary uncertainties in the present calculations stem from the recipes of stellar wind, remnant formation and their natal kicks, that are adopted here (Sec. 2.2). Although such recipes can, in a sense, be called the state-of-the-art because of their relatively popular applications in the literature, nearly all aspects of stellar remnant formation (especially of BH formation; see Sec. 2.2) remain poorly understood or constrained to date. These uncertainties translate into those in the BHs' mass spectrum and initial retention in stellar clusters. Another factor that might have affected the current results to some extent is the lack of primordial binaries, which is done to make these computations feasible. Although Monte-Carlo calculations of much more massive clusters indicate near indifference of the BH dynamics to the presence of primordial binaries (Sec. 2.3 and references therein), the situation can be different for lower mass systems, where the dynamical interactions are generally less energetic. Furthermore, mass transfer and/or tidal interactions among massive-stellar and close primordial binaries would influence the masses of the BHs (Thomas Tauris, Philipp Podsiadlowski, private communications; see also De Mink et al. 2009; Marchant et al. 2016 in this context). Moreover, dynamically induced (Banerjee et al. 2012) or mass-transfer driven (De Mink et al. 2014) coalescences of massive-stellar binaries would form more massive merger products, which would yield more massive BHs.

The immediate next step would be to obtain an even more exhaustive set of model calculations by reaching even higher $M_{\text{cl}}(0)$ s and obtaining more evolutionary models for the lowest cluster masses (and perhaps explore even lower masses). These will also help to understand better the role of BH subsystems and their impact on the parent cluster's dynamics and BBH coalescence events, as discussed above and in the previous sections. Inclusion of primordial binaries would be feasible at least for the least-massive systems, which would be intriguing to do. Such steps are planned by the author for the near future.

ACKNOWLEDGEMENTS

The author is indebted to Sverre Aarseth of the Institute of Astronomy, Cambridge, for his continuous efforts in improving NBODY6/7, without which this study wouldn't have been possible. SB is thankful to Jarrod Hurley of the Swinburne University of Technology for reviewing the changes made in the BSE's routines for this work, testing them independently, and also for interesting discussions. SB is thankful to Chris Belczynski of the Astronomical Observatory, University of Warsaw, for supplying the data corresponding to the ZAMS

mass-remnant mass relations, as obtained from the StarTrack program (Fig. 1), and also for useful discussions. SB is thankful to the anonymous referee for helpful comments that improved some of the descriptions of the paper. Finally, but not the least, SB is indebted to the computing team of the Argelander-Institut für Astronomie, University of Bonn, for their support and efficient maintenance of the workstations on which all the computations have been performed.

References

- Aarseth S. J., 2003, Gravitational N-Body Simulations
Aarseth S. J., 2012, *MNRAS*, **422**, 841
Abbott B. P., et al., 2016a, *Physical Review Letters*, **116**, 061102
Abbott B. P., et al., 2016b, *Physical Review Letters*, **116**, 241103
Abbott B. P., et al., 2016c, *ApJ*, **818**, L22
Alessandrini E., Lanzoni B., Ferraro F. R., Mocchi P., Vesperini E., 2016, *ApJ*, **833**, 252
Antonini F., Rasio F. A., 2016, *ApJ*, **831**, 187
Arca-Sedda M., 2016, *MNRAS*, **455**, 35
Askar A., Szkudlarek M., Gondek-Rosińska D., Giersz M., Bulik T., 2016, *Monthly Notices of the Royal Astronomical Society: Letters*, **464**, L36
Banerjee S., Kroupa P., 2015a, preprint, ([arXiv:1512.03074](https://arxiv.org/abs/1512.03074))
Banerjee S., Kroupa P., 2015b, *MNRAS*, **447**, 728
Banerjee S., Kroupa P., 2016, *A&A*, **597**, A28
Banerjee S., Baumgardt H., Kroupa P., 2010, *MNRAS*, **402**, 371
Banerjee S., Kroupa P., Oh S., 2012, *MNRAS*, **426**, 1416
Belczynski K., Kalogera V., Bulik T., 2002, *The Astrophysical Journal*, **572**, 407
Belczynski K., Kalogera V., Rasio F. A., Taam R. E., Zezas A., Bulik T., Maccarone T. J., Ivanova N., 2008, *The Astrophysical Journal Supplement Series*, **174**, 223
Belczynski K., Bulik T., Fryer C. L., Ruiter A., Valsecchi F., Vink J. S., Hurley J. R., 2010, *The Astrophysical Journal*, **714**, 1217
Belczynski K., Holz D. E., Bulik T., O'Shaughnessy R., 2016, *Nature*, **534**, 512
Bovill M. S., Puzia T. H., Ricotti M., Taylor M. A., 2016, *ApJ*, **832**, 88
Breen P. G., Heggie D. C., 2013a, *Monthly Notices of the Royal Astronomical Society*, **432**, 2779
Breen P. G., Heggie D. C., 2013b, *Monthly Notices of the Royal Astronomical Society*, **436**, 584
Brem P., Amaro-Seoane P., Spurzem R., 2013, *MNRAS*, **434**, 2999
Campanelli M., Lousto C., Zlochower Y., Merritt D., 2007, *ApJ*, **659**, L5
Chatterjee S., Rodriguez C. L., Rasio F. A., 2016a, preprint, ([arXiv:1603.00884](https://arxiv.org/abs/1603.00884))
Chatterjee S., Rodriguez C. L., Kalogera V., Rasio F. A., 2016b, preprint, ([arXiv:1609.06689](https://arxiv.org/abs/1609.06689))
De Mink S. E., Cantiello M., Langer N., Pols O. R., Brott I., Yoon S.-C., 2009, *A&A*, **497**, 243
De Mink S. E., Sana H., Langer N., Izzard R. G., Schneider F. R. N., 2014, *ApJ*, **782**, 7
Downing J. M. B., Benacquista M. J., Giersz M., Spurzem R., 2010, *Monthly Notices of the Royal Astronomical Society*, **407**, 1946
Downing J. M. B., Benacquista M. J., Giersz M., Spurzem R., 2011, *Monthly Notices of the Royal Astronomical Society*, pp no–no
Fryer C. L., 1999, *The Astrophysical Journal*, **522**, 413
Fryer C. L., Kalogera V., 2001, *The Astrophysical Journal*, **554**, 548
Gieles M., Larsen S. S., Scheepmaker R. A., Bastian N., Haas M. R., Lamers H. J. G. L. M., 2006a, *A&A*, **446**, L9

- Gieles M., Larsen S. S., Bastian N., Stein I. T., 2006b, *A&A*, **450**, 129
- Hansen B. M. S., Phinney E. S., 1997, *Monthly Notices of the Royal Astronomical Society*, **291**, 569
- Haster C.-J., Antonini F., Kalogera V., Mandel I., 2016, *ApJ*, **832**, 192
- Heggie D. C., 1975, *MNRAS*, **173**, 729
- Heggie D., Hut P., 2003, The Gravitational Million-Body Problem: A Multidisciplinary Approach to Star Cluster Dynamics
- Hénon M., 1975, in Hayli A., ed., IAU Symposium Vol. 69, Dynamics of the Solar Systems. p. 133
- Hobbs G., Lorimer D. R., Lyne A. G., Kramer M., 2005, *MNRAS*, **360**, 974
- Hughes S. A., 2009, *ARA&A*, **47**, 107
- Hurley J. R., Pols O. R., Tout C. A., 2000, *Monthly Notices of the Royal Astronomical Society*, **315**, 543
- Hurley J. R., Tout C. A., Pols O. R., 2002, *Monthly Notices of the Royal Astronomical Society*, **329**, 897
- Hurley J. R., Sippel A. C., Tout C. A., Aarseth S. J., 2016, *Publ. Astron. Soc. Australia*, **33**, e036
- Johnson K. E., Leroy A. K., Indebetouw R., Brogan C. L., Whitmore B. C., Hibbard J., Sheth K., Evans A. S., 2015, *ApJ*, **806**, 35
- Kimpson T. O., Spera M., Mapelli M., Ziosi B. M., 2016, *MNRAS*, **463**, 2443
- Kozai Y., 1962, *The Astronomical Journal*, **67**, 591
- Kroupa P., Weidner C., Pflamm-Altenburg J., Thies I., Dabringhausen J., Marks M., Maschberger T., 2013, The Stellar and Sub-Stellar Initial Mass Function of Simple and Composite Populations. p. 115, doi:10.1007/978-94-007-5612-0_4
- Kulkarni S. R., Hut P., McMillan S., 1993, *Nature*, **364**, 421
- Larsen S. S., 2009, *Astronomy and Astrophysics*, **494**, 539
- Longmore S. N., et al., 2014, *Protostars and Planets VI*, pp 291–314
- Mackey A. D., Wilkinson M. I., Davies M. B., Gilmore G. F., 2007, *MNRAS*, **379**, L40
- Mackey A. D., Wilkinson M. I., Davies M. B., Gilmore G. F., 2008, *MNRAS*, **386**, 65
- Mapelli M., Zampieri L., Ripamonti E., Bressan A., 2013, *MNRAS*, **429**, 2298
- Marchant P., Langer N., Podsiadlowski P., Tauris T. M., Moriya T. J., 2016, *A&A*, **588**, A50
- Mikkola S., Aarseth S. J., 1993, *Celestial Mechanics & Dynamical Astronomy*, **57**, 439
- Mikkola S., Merritt D., 2008, *The Astronomical Journal*, **135**, 2398
- Mikkola S., Tanikawa K., 1999, *Monthly Notices of the Royal Astronomical Society*, **310**, 745
- Miller-Jones J. C. A., et al., 2015, *Mon. Not. R. Astron. Soc.*, **453**, 3919
- Morscher M., Pattabiraman B., Rodriguez C., Rasio F. A., Umbreit S., 2015, *The Astrophysical Journal*, **800**, 9
- Nitadori K., Aarseth S. J., 2012, *Monthly Notices of the Royal Astronomical Society*, **424**, 545
- Peters P. C., 1964, *Physical Review*, **136**, 1224
- Peuten M., Zocchi A., Gieles M., Gualandris A., Hénauld-Brunet V., 2016, *MNRAS*, **462**, 2333
- Podsiadlowski P., Langer N., Poelarends A. J. T., Rappaport S., Heger A., Pfahl E., 2004, *The Astrophysical Journal*, **612**, 1044
- Portegies Zwart S. F., McMillan S. L. W., 2000, *ApJ*, **528**, L17
- Portegies Zwart S. F., McMillan S. L. W., Gieles M., 2010, *ARA&A*, **48**, 431
- Renaud F., Gieles M., 2015, *MNRAS*, **449**, 2734
- Renaud F., et al., 2015, *MNRAS*, **454**, 3299
- Rodriguez C. L., Morscher M., Pattabiraman B., Chatterjee S., Haster C.-J., Rasio F. A., 2015, *Phys. Rev. Lett.*, **115**
- Rodriguez C. L., Chatterjee S., Rasio F. A., 2016a, *Physical Review D*, **93**
- Rodriguez C. L., Haster C.-J., Chatterjee S., Kalogera V., Rasio F. A., 2016b, *ApJ*, **824**, L8
- Rubio M., Elmegreen B. G., Hunter D. A., Brinks E., Cortés J. R., Cigan P., 2015, *Nature*, **525**, 218
- Ryon J. E., et al., 2015, *MNRAS*, **452**, 525
- Sana H., Evans C. J., 2011, in Neiner C., Wade G., Meynet G., Peters G., eds, IAU Symposium Vol. 272, Active OB Stars: Structure, Evolution, Mass Loss, and Critical Limits. pp 474–485 (arXiv:1009.4197), doi:10.1017/S1743921311011124
- Sana H., et al., 2013, *A&A*, **550**, A107
- Sánchez Almeida J., et al., 2015, *ApJ*, **810**, L15
- Sigurdsson S., Hernquist L., 1993, *Nature*, **364**, 423
- Sippel A. C., Hurley J. R., 2013, *MNRAS*, **430**, L30
- Sollima A., et al., 2016, *MNRAS*, **462**, 1937
- Spera M., Mapelli M., Bressan A., 2015, *Mon. Not. R. Astron. Soc.*, **451**, 4086
- Spitzer L., 1987, Dynamical evolution of globular clusters
- Strader J., Chomiuk L., Maccarone T. J., Miller-Jones J. C. A., Seth A. C., 2012, *Nature*, **490**, 71
- Taylor M. A., Puzia T. H., Gomez M., Woodley K. A., 2015, *ApJ*, **805**, 65
- Vink J. S., de Koter A., 2005, *Astronomy and Astrophysics*, **442**, 587
- Vink J. S., de Koter A., Lamers H. J. G. L. M., 2001, *Astronomy and Astrophysics*, **369**, 574
- Wang L., Spurzem R., Aarseth S., Nitadori K., Berczik P., Kouwenhoven M. B. N., Naab T., 2015, *Monthly Notices of the Royal Astronomical Society*, **450**, 4070
- Wang L., et al., 2016, *Mon. Not. R. Astron. Soc.*, **458**, 1450
- Weidner C., Kroupa P., 2004, *MNRAS*, **348**, 187
- Wright E. L., 2006, *PASP*, **118**, 1711
- Ziosi B. M., Mapelli M., Branchesi M., Tormen G., 2014, *MNRAS*, **441**, 3703